Drosophila CLIP-190 and mammalian CLIP-170 display reduced microtubule plus end association in the nervous system

Drosophila CLIP-190 and mammalian CLIP-170 display reduced microtubule plus end association in the nervous system

Robin Beaven[a,*], Nikola S. Dzhindzhev[b,†], Yue Qu[a], Ines Hahn[a], Federico Dajas-Bailador[a,‡], Hiroyuki Ohkura[b], and Andreas Prokop[a]

[a]Faculty of Life Sciences, The University of Manchester, Manchester M13 9PT, United Kingdom; [b]Wellcome Trust Centre for Cell Biology, Institute of Cell Biology, School of Biological Sciences, University of Edinburgh, Edinburgh EH9 3JR, United Kingdom

ABSTRACT **Axons act like cables, electrically wiring the nervous system. Polar bundles of microtubules (MTs) form their backbones and drive their growth. Plus end–tracking proteins (+TIPs) regulate MT growth dynamics and directionality at their plus ends. However, current knowledge about +TIP functions, mostly derived from work in vitro and in nonneuronal cells, may not necessarily apply to the very different context of axonal MTs. For example, the CLIP family of +TIPs are known MT polymerization promoters in nonneuronal cells. However, we show here that neither *Drosophila* CLIP-190 nor mammalian CLIP-170 is a prominent MT plus end tracker in neurons, which we propose is due to low plus end affinity of the CAP-Gly domain–containing N-terminus and intramolecular inhibition through the C-terminus. Instead, both CLIP-190 and CLIP-170 form F-actin–dependent patches in growth cones, mediated by binding of the coiled-coil domain to myosin-VI. Because our loss-of-function analyses in vivo and in culture failed to reveal axonal roles for CLIP-190, even in double-mutant combinations with four other +TIPs, we propose that CLIP-190 and -170 are not essential axon extension regulators. Our findings demonstrate that +TIP functions known from nonneuronal cells do not necessarily apply to the regulation of the very distinct MT networks in axons.**

Monitoring Editor
Erika Holzbaur
University of Pennsylvania

Received: Jun 12, 2014
Revised: Jan 5, 2015
Accepted: Feb 10, 2015

INTRODUCTION

Axons are the cable-like neuronal protrusions that electrically wire the nervous system. The structural backbones of axons are polar bundles of microtubules (MTs) oriented with their plus ends toward the distal axon tips. MTs grow and shrink at their plus ends, and their positive net polymerization is believed to drive MT bundle extension and hence axon growth (Conde and Caceres, 2009; Dent *et al.*, 2011; Prokop, 2013; Prokop *et al.*, 2013). End-binding proteins (EBs) directly bind to MT plus ends and recruit other plus end–tracking proteins (+TIPs) to this position (Akhmanova and Steinmetz, 2008, 2010; Etienne-Manneville, 2010). These various +TIPs are proposed to determine MT growth, shrinkage, targeting, and stability. However, experimental support for such roles of +TIPs during axon growth remains patchy, not least due to the fact that different +TIP members display functional redundancies.

The +TIPs are evolutionarily well conserved, and the fruit fly *Drosophila* provides powerful means for their study, enormously facilitated by low genetic redundancy and high amenability to genetic manipulations (Sánchez-Soriano *et al.*, 2007; Prokop *et al.*, 2013). Roles for some fly +TIPs during axon growth have been demonstrated. For example, *Drosophila* cytoplasmic linker-associated protein (dCLASP) acts in axonal midline guidance (Lee *et al.*, 2004; Lowery *et al.*, 2010), and fly EB1 promotes axon growth in part through evolutionarily conserved MT-organizing functions of

This article was published online ahead of print in MBoC in Press (http://www.molbiolcell.org/cgi/doi/10.1091/mbc.E14-06-1083) on February 18, 2015.

Present addresses: *Wellcome Trust Centre for Cell Biology, Institute of Cell Biology, School of Biological Sciences, University of Edinburgh, Edinburgh EH9 3JR, United Kingdom; †Department of Genetics, University of Cambridge, Cambridge CB2 3EH, United Kingdom; ‡School of Biomedical Sciences, University of Nottingham, Medical School, Queen's Medical Centre, Nottingham NG7 2UH, United Kingdom.

The authors declare no competing financial interests.

Address correspondence to: Andreas Prokop (Andreas.Prokop@manchester.ac.uk).

Abbreviations used: CLIP, cytoplasmic linker protein; EB, end-binding protein; GC, growth cone; MT, microtubule; +TIP, microtubule plus end–tracking protein.

Supplemental Material can be found at:
http://www.molbiolcell.org/content/suppl/2015/02/16/mbc.E14-06-1083v1.DC1.html

the +TIP Short stop (Shot; Sánchez-Soriano *et al.*, 2009; Alves-Silva *et al.*, 2012).

Here we capitalized on experimentally and genetically amenable fly neurons to test the axonal functions of another +TIP family, the CAP-Gly domain–containing/cytoplasmic linker proteins (CLIPs). Previous primary neuron work suggested that mammalian CLIP-170 enhances dendrite growth (Swiech *et al.*, 2011) and, together with its paralogue CLIP-115, promotes axon growth (Neukirchen and Bradke, 2011). However, CLIP-170/115 double-knockout mice are viable (Miedema, 2007), leaving uncertainty about their nervous system functions in vivo. In *Drosophila*, the only family member is CLIP-190, which contains a carboxy terminus that is also present in vertebrate CLIP-170 but absent in CLIP-115 (De Zeeuw *et al.*, 1997). Like vertebrate CLIPs, *Drosophila* CLIP-190 forms EB1-dependent comets in cultured interphase cells (Dzhindzhev *et al.*, 2005), where it promotes MT recovery after cold treatment (Rogers *et al.*, 2008). Of note, CLIP-190 is enriched in the developing nervous system (Lantz and Miller, 1998), but its roles in this tissue have not yet been assessed.

Here we found that CLIP-190 in fly neurons significantly deviates from its behavior in nonneuronal cells, and similar observations were made for mammalian CLIP-170 in mouse neurons. Both showed low MT plus end localization, which we suggest is dependent on both low affinity of the N-terminus and intramolecular inhibition through the C-terminus. Both localized as static myosin-VI– and F-actin–dependent patches in the center of growth cones. Furthermore, we found that complete loss-of-function mutants of CLIP-190, alone or in double-mutant combinations with four other +TIPs, failed to reveal aberrations in axon growth in vivo and in culture, suggesting that CLIP-190 (and potentially also CLIP-170) does not possess a significant role in the axon growth–promoting MT machinery.

RESULTS

CLIP-190 is not a prominent MT plus end tracker in the nervous system

Drosophila CLIP-190 was highly enriched in the embryonic nervous system, forming punctate accumulations (Lantz and Miller, 1998). To understand this localization and its potential functional relevance, we first looked at embryos at stage 16 (a midembryonic stage at which rudimentary neuronal circuits are established but axons are still growing; Campos-Ortega and Hartenstein, 1997). We used an anti–CLIP-190 antibody that was previously used in S2 cells, where it localizes to MT plus ends in an EB1-dependent manner (Dzhindzhev *et al.*, 2005). In stage 16 embryos, we found that CLIP-190 protein was particularly enriched in the neuropile, that is, the central region of the CNS, which exclusively contains axons (Sánchez-Soriano *et al.*, 2007; Figure 1A). In the neuropile, CLIP-190 occurred in broad patches (1.6 µm ± 0.07 SEM average diameter; $n = 65$; Figure 1B). In contrast, nonneuronal tissues in the same embryos showed dashes of staining that were narrow (0.34-µm width) and more likely to represent MT plus end comets (Figure 1E).

We corroborated our findings using targeted expression of green fluorescent protein (GFP)::CLIP-190. In nonneuronal cells and tissues, such as hemocytes, epidermis, and amnioserosa, GFP::CLIP-190 performed highly dynamic MT plus end tracking, consistent with our anti–CLIP-190 antibody staining (Figures 1, D–F, and 2, C and D). However, in the nervous system, the same GFP::CLIP-190 predominantly formed broad patches (1.7 µm ± 0.07 SEM average diameter; $n = 66$), and, in fixed embryos, these patches fully overlapped with anti-CLIP-190–stained accumulations (Figure 1C). Live analyses with GFP::CLIP-190 revealed that these patches in the CNS neuropile displayed hardly any dynamics, and only occasional slow movements over a few micrometers were observed (Figure 2A and Supplemental Movie S1). Of note, we also observed that overexpression induced stable patches in nonneuronal cells—for example, in the amnioserosa or at the leading edge of dorsal epidermal cells (Figures 1F and 2D). Our data suggest that patch formation is a predominant phenomenon in neurons but that nonneuronal cells can, in principle, show similar behaviors (see *Discussion*).

To study the subcellular localization of these patches, we used primary embryonic *Drosophila* neurons in culture, which provide the required resolution (Sánchez-Soriano *et al.*, 2010; Prokop *et al.*, 2012). In almost all primary neurons, antibody staining revealed patches of endogenous CLIP-190. These patches localized to the center of growth cones in 96% of neurons and to axon shafts in 19% of neurons ($n = 74$; Figure 1G). The patches in culture were larger than observed in vivo (average diameter, 3.6 µm ± 0.2 SEM; $n = 67$), and this is expected because growth cones (GCs) tend to spread out on glass, whereas most GCs in vivo are likely to adhere to narrow fiber tracts, which are well established at this stage (Sánchez-Soriano and Prokop, 2005). GFP::CLIP-190 displayed the same growth cone patches in cultured neurons, which were similarly static, like those observed in vivo (Figure 2, A–B′). Endogenous and GFP-tagged CLIP-190 showed very rarely detectable comet localization, which was always far weaker than the prominent comets displayed in nonneuronal cell types. Of note, other +TIPs, such as EB1 (endogenous and GFP-tagged) and dCLASP (GFP-tagged), form prominent comets in these neurons (Alves-Silva *et al.*, 2012; see later discussion), and we draw two conclusions. First, lack of comet formation in neurons is a specific feature of CLIP-190 rather than a general phenomenon of neuronal +TIPs. Second, CLIP-190 displays a far lower propensity to localize to EB1 at MT plus ends in neurons than in nonneuronal cells and displays an atypical tendency to bind to other, unknown factors, forming patch-like accumulations primarily in growth cones.

CLIP-190 patch localization in GCs is conserved with mammalian CLIP-170

The closest mammalian homologue of CLIP-190 is CLIP-170 (Lantz and Miller, 1998). Our literature searches suggested that localization of endogenous CLIP-170 in neurons has not been reported, but overexpression of GFP::CLIP-170 or antisera detecting both CLIP-115 and CLIP-170 had been used instead (see *Discussion*). We therefore tested whether the atypical localization of CLIP-190 in neurons might be evolutionarily conserved with CLIP-170.

For this, we used anti–CLIP-170 antiserum (sc-25613) to stain mouse cortical neurons at 3 d in vitro (DIV) and found strong patch localization in GCs of 89% of neurons ($n = 47$; Figure 3A). In contrast, parallel staining in nonneuronal cells with the same antiserum showed prominent comet structures at MT plus ends, consistent with previous reports (Figure 3E; compare Rickard and Kreis, 1990; Komarova *et al.*, 2002; Goodson *et al.*, 2003; Lee *et al.*, 2010). To further validate our finding, we used transfection of mouse cortical neurons with GFP::CLIP-170. For this, we used the AJ237670 isoform of CLIP-170 (GenBank), which is the most prevalent in rat brain (A. Akhmanova, personal communication). Accordingly, our reverse transcription PCR analyses revealed that Clip1-003 (Ensembl), which is virtually identical to AJ237670, is also the most abundant isoform in mouse cortical primary neurons (Supplemental Figure S2 and Supplemental Table S1). When AJ237670-derived GFP::CLIP-170 was expressed in nonneuronal NIH/3T3 fibroblasts, we observed prominent MT plus end tracking (Figure 3F). The same construct expressed in cortical mouse neurons reproduced the large GC patches found for endogenous protein (46% of neurons; $n = 32$;

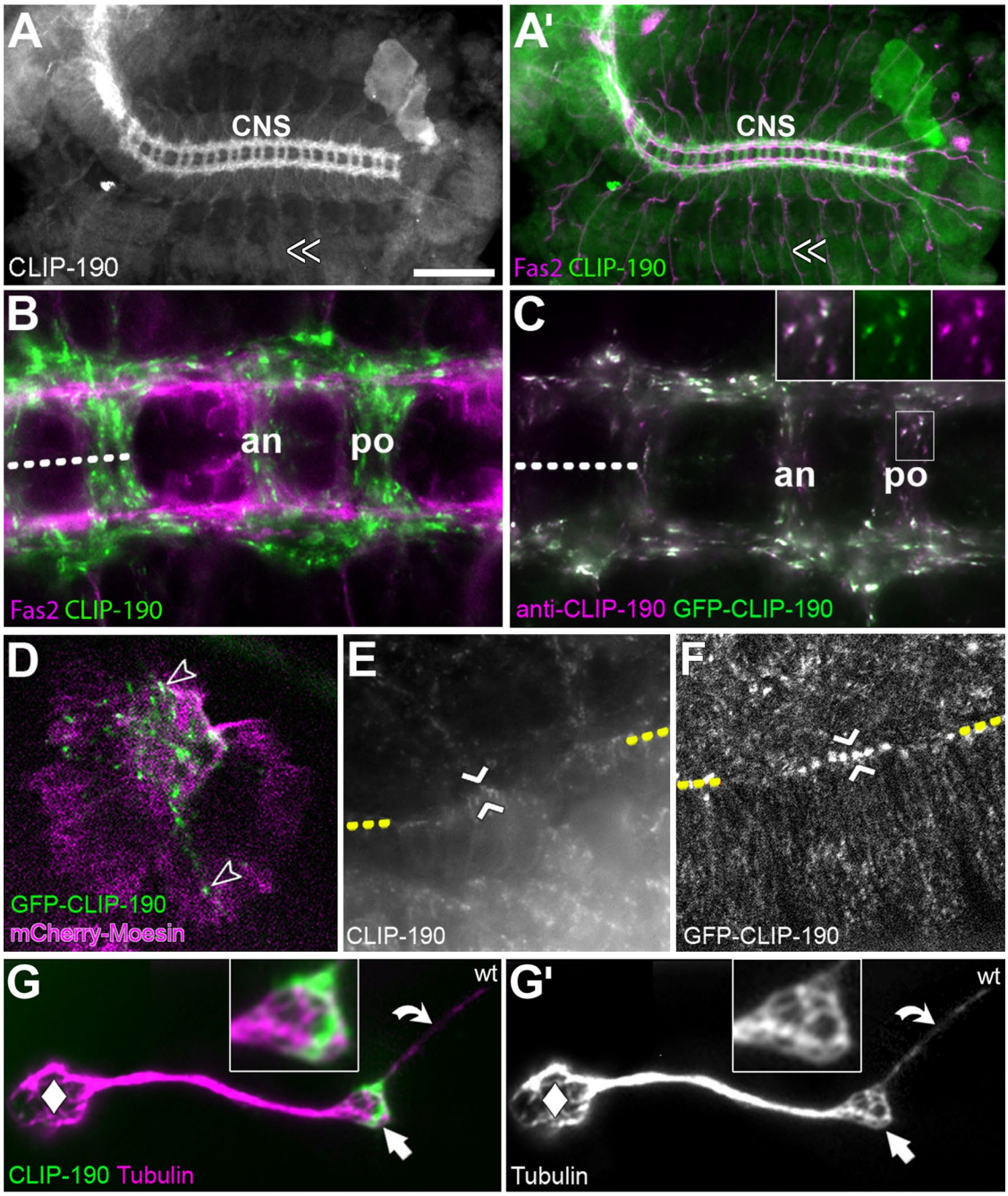

FIGURE 1: CLIP-190 localizes predominantly as stable accumulations in growing neurons. (A) In stage 16 embryo, CLIP-190 (green) is particularly enriched in the ladder-like axonal neuropile of the CNS (colabeled with Fas2 in magenta; double chevrons point at motor nerves). (B, C) Higher magnification of stage 16 neuropiles shows that endogenous CLIP-190 and GFP::CLIP-190 localize into prominent patches; CNS midlines (stippled lines) and anterior (an) and posterior (po) commissures are indicated; boxed area in C is shown 2× magnified in insets at the top, which display the two channels combined and alone. (D) Still image from a live movie of a hemocyte in a *Drosophila* embryo visualized for mCherry::moesin (magenta; indicating F-actin) and GFP::CLIP-190 (green); GFP::CLIP-190 forms abundant prominent comets (open arrowhead). (E) In outer epithelia (amnioserosa, above stippled line; epidermis, below stippled line) of fixed stage 15 embryos, endogenous CLIP-190 localizes to small puncta, which are enriched at cell perimeters, including the leading edge of the dorsal epidermis (between chevrons). (F) Live imaging with GFP::CLIP-190 (one still image shown) revealed prominent comets in the amnioserosa and slightly weaker comets in the epidermis, suggesting that puncta in E are comets; GFP::CLIP-190 localized to large stable accumulations at the leading edge of the epidermis (between chevrons) which are in the same position as dMyoVI reported previously (Millo *et al.*, 2004). (G) In embryo-derived primary neurons after 6 h in culture, endogenous CLIP-190 (green) localizes into prominent patches in GCs (arrow) that do not correlate with MTs (diamond indicates the cell body, curved arrow a single MT in a filopodium). Scale bar in A represents 100 µm (A), 10 µm (B, C), 15 µm (D), 40 µm (E, F), 5 µm (G).

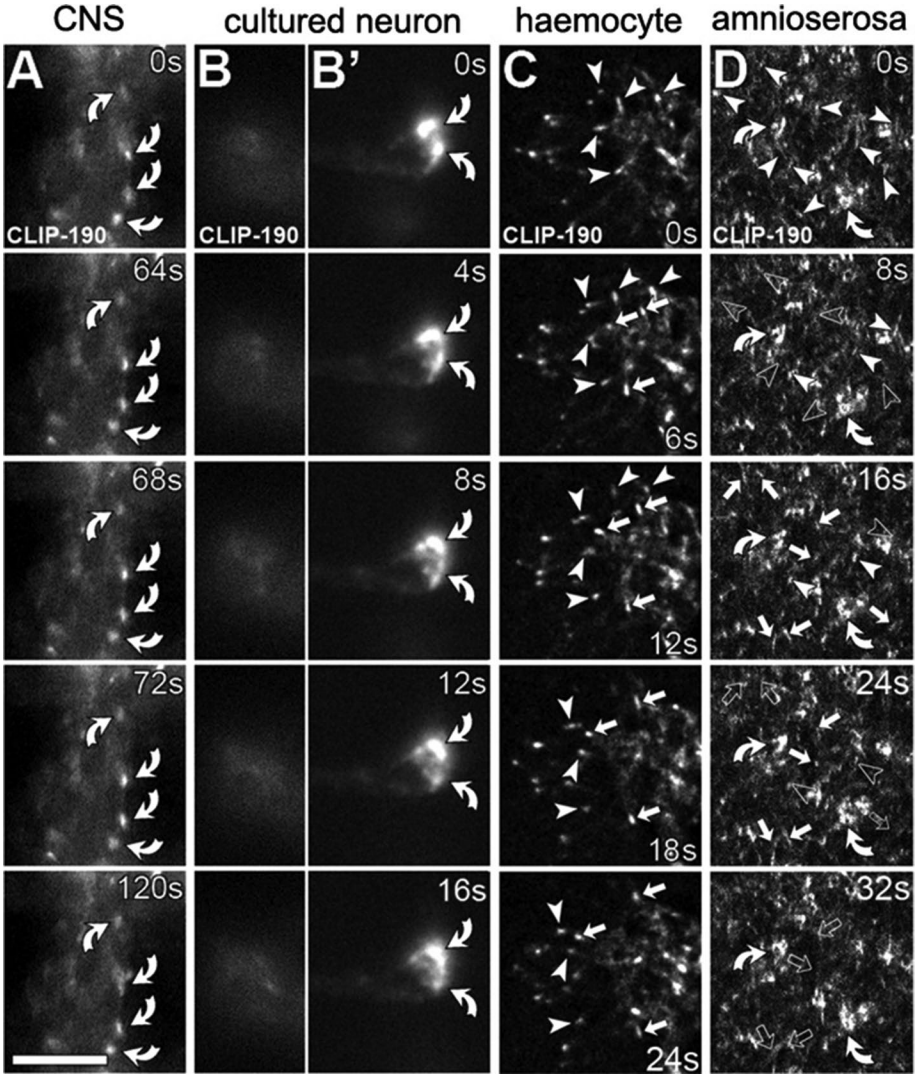

FIGURE 2: CLIP dynamics is cell-type specific and partially regulated through autoinhibition in neurons. Columns show series of stills from time-lapse movies of different cells or tissues expressing GFP::CLIP-190 (time intervals indicated at right). (A) Embryonic *Drosophila* CNS at stage 16 (close-up of one commissure; compare Figure 1); GFP::CLIP-190 localizes to patches displaying little movement over 2 min (curved arrows). (B, B′) *Drosophila* primary neuron cultured for 6 h; GFP::CLIP-190 lacks moving comets in cell body (B) and axon/GC (B′), and the prominent GC patch shows little movement. (C) In hemocytes (blood cells) of embryos in vivo, GFP::CLIP-190 displays prominent MT tip tracking (arrowheads and arrows). (D) In the embryonic amnioserosa (compare Figure 1F), most MTs move perpendicular to the imaging plain, and comets are difficult to track; GFP::CLIP-190 dots appear transiently (white arrowheads and arrows) and vanish soon after (open arrowheads and arrows), indicating that comets reaching the imaging plain are dynamic; however, overexpression of GFP::CLIP-190 also causes more stable patches, reminiscent of GC patches in GCs (curved arrows). Scale bar in A represents 12 µm (A), 5 µm (B, B′), 15 µm (C), 34 µm (D).

Figure 3, B and D). Unlike endogenous protein, it also formed dynamic comets in virtually all neurons, although these appeared fainter than observed in nonneuronal cells. Of note, the GFP::CLIP-170 comets were also picked up by anti–CLIP-170 antibodies in fixed cells, whereas untransfected neurons in the same culture dish never displayed MT plus end localization (Figure 3C).

Therefore endogenous mouse CLIP-170 also displays prominent patch localization in growth cones and a lower propensity to localize to MT plus ends than in nonneuronal cells, suggesting that these neuron-specific behaviors are evolutionarily conserved with *Drosophila* CLIP-190.

Other +TIPs have no detectable effect on the MT plus end localization of CLIP-190

We then sought to understand what molecular mechanisms underlie this atypical localization of CLIPs in the neuronal context. We first tested whether other +TIPs might negatively effect CLIP-190 comet formation. They could do so by competing CLIP-190 away from the limited pool of EB1 at MT plus ends or through direct molecular interactions such as the known binding of CLIP-170/190 to CLASP, to the dynein/dynactin-associated protein Lis1, or to Glued (Akhmanova *et al.*, 2001; Coquelle *et al.*, 2002; Goodson *et al.*, 2003; Mathe *et al.*, 2003; Weisbrich *et al.*, 2007).

We therefore tested potential roles of these three candidates plus two further designated +TIPs, Apc and Shot. We started by assessing their expression and localization in *Drosophila* neurons. First, dCLASP (officially called Chromosome bows/Chb) is the only *Drosophila* CLASP family member, and its functional loss causes guidance defects at the CNS midline (Lee *et al.*, 2004). Accordingly, we found that dCLASP behaves like a prominent +TIP, localizing as dynamic comets, as we observe for EB1 (Figure 4, A and B). For dCLASP, these comets are primarily seen in GCs, as similarly reported for frog and mouse neurons (Figure 4C; Lee *et al.*, 2004; Hur *et al.*, 2011). Second, lissencephaly-1 (Lis-1) is its only family member in *Drosophila* and is required in vivo for correct photoreceptor axon path finding and dendrite growth (Liu *et al.*, 2000; Marrone *et al.*, 2011). We found that fly Lis1 distributes throughout GCs (Figure 4F), similar to reports in vertebrate neurons (Grabham *et al.*, 2007; Moughamian *et al.*, 2013). Third, dynactin 1 (also known as p150 or Glued) is an interactor of EB1 and forms part of the dynein/dynactin motor complex (Allan, 2011; Prokop, 2013), and *Drosophila* Glued is required for axon growth in vivo (Murphey *et al.*, 1999). Unfortunately, no tools were available to us to assess its neuronal localization. Fourth, two adenomatous polyposis coli (APC) proteins (Apc, Apc2) exist in flies, of which Apc is EB1 binding (Mattie *et al.*, 2010). In vivo studies using combined loss of both APCs failed to yield obvious nervous system defects (Rusan *et al.*, 2008), although we found strong Apc expression in neurons, where it tends to form immobile accumulations positioned along MTs in a selective subregion of GCs (Figure 4, D and E). This pattern is reminiscent of vertebrate APC in neurons and nonneuronal cells alike (Näthke *et al.*, 1996; Zhou *et al.*, 2004; Votin *et al.*, 2005; Garrido *et al.*, 2007; Koester *et al.*, 2007). Finally, Shot is the only *Drosophila* spectraplakin, regulates axon growth through interaction with EB1, and was previously shown to localize to MTs in GCs (Sánchez-Soriano *et al.*, 2009; Alves-Silva *et al.*, 2012).

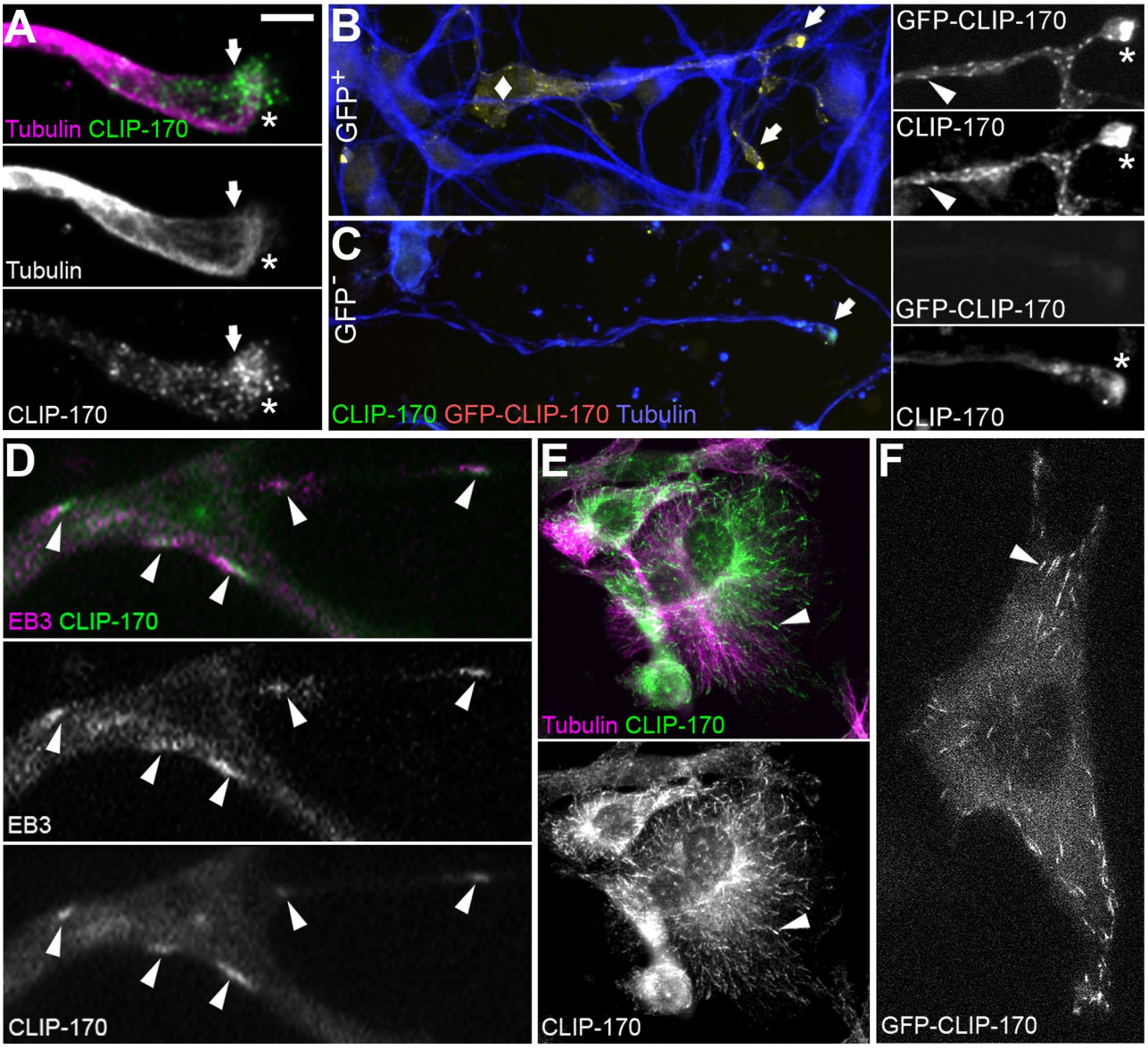

FIGURE 3: CLIP-170 localizes as GC patches in mouse cortical neurons. (A) In cultured mouse cortical neurons after 4 DIV, endogenous CLIP-170 accumulates in patches (asterisk) within GCs (arrow). (B) In GFP::CLIP-170–expressing neurons, GFP (top close-up; twofold magnified) and anti–CLIP-170 staining (bottom close-up) display patches and MT plus end localization (arrowheads); diamond indicates a neuronal cell soma. (C) In untransfected neurons on the same culture dish, endogenous CLIP-170 can only be seen in patches in GCs. (D) In transfected cortical neurons imaged live, GFP::CLIP-170 (CLIP-170) is frequently seen as dynamic comet structures that colocalize with mRFP::EB3 (EB3) comets (arrowhead). A section of axon is shown. (E) Anti-CLIP-170 staining in mouse EpH4 epithelial cells shows clear localization as comets (e.g., arrowhead); fixed with methanol/EGTA followed by PFA postfixation (see *Materials and Methods*). (F) Still image from live imaging of mouse NIH/3T3 fibroblasts showing predominantly comet localization of GFP::CLIP-170 when expressing at low levels (e.g., arrowhead). Scale bar in A represents 5 µm (A), 15 µm (B, C, E), 2.75 µm (D), 7.5 µm (F).

Having convinced ourselves of the presence of these designated +TIPs in *Drosophila* neurons, we then analyzed mutant alleles known to abolish their functions (*chb*^{2}, *Apc*^{Q8} *Apc2*^{g10} double mutant, Gl$^{\Delta 22}$, *shot*^{3}, and *lis1*^{K13209}; see *Materials and Methods*). Surprisingly, homozygosis for any of these mutations in *Drosophila* neurons failed to cause up-regulation of CLIP-190 at MT plus ends, loss of GC patch localization, or any other obvious change in the distribution pattern of endogenous CLIP-190 (Figure 4, G–L). This finding suggests that interaction with other +TIPs is not a likely cause for the atypical localization of CLIP-170/190 in neurons.

Patch localization of CLIPs is mediated by dMyoVI and F-actin

A further interaction of CLIP-190 has been suggested to occur with the *Drosophila* myosin-VI homologue Jaguar (Jar; here referred to as dMyoVI; Lantz and Miller, 1998). We therefore tested whether this link is functionally relevant and might explain the atypical behavior of CLIP-190 in neurons. First, we used antibody staining against endogenous dMyoVI protein, as well as neuronal expression of GFP-tagged isoforms. In *Drosophila* primary neurons, we found that dMyoVI also displays prominent patches in the center of GCs

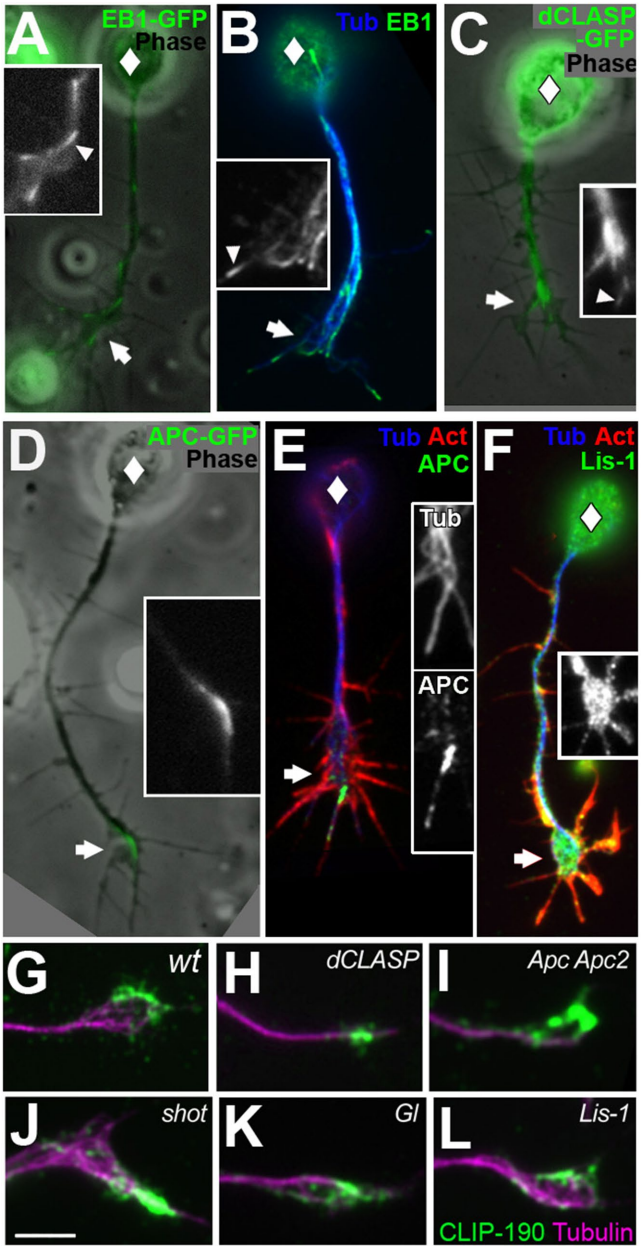

FIGURE 4: Localization of +TIPs in *Drosophila* neurons. All images show *Drosophila* primary neurons at 6 h in culture. (A) Still image from a time-lapse movie of an EB1::GFP–expressing neuron, which forms dynamic comets (arrowheads in inset) throughout the neuron. (B) Endogenous EB1 (green) in a fixed neuron costained for tubulin (blue) reproduces the localization pattern of EB1::GFP. (C) Still image from live imaging of a dCLASP::GFP–expressing neuron, which forms dynamic comets (arrowheads in inset) primarily in GCs. (D) Live imaging of Apc::GFP shows prominent, mostly immobile accumulations usually selectively in one subregion of GCs, along MTs. (E) Endogenous Apc (green) in a fixed neuron costained for tubulin (blue) and F-actin (red) reproduces the localization pattern of Apc::GFP and clearly shows that APC localizes at MTs. (F) Endogenous Lis-1 (green) in a fixed neuron costained for tubulin (blue) and F-actin (red) shows GC enrichment. In A, C, and D, phase contrast shows neuron morphology. (G–L) GC patch localization of endogenous CLIP-190 (G, wild-type control) is not affected in primary neurons carrying the following mutant constellations: (H) *dCLASP*$^{2/2}$, (I) *APC2*$^{g10/g10}$, *APC1*$^{Q8/Q8}$, (J) *shot*$^{3/3}$, (K) *Gl*$^{\Delta 22/\Delta 22}$, and (L) *lis1*$^{K13209/K13209}$. Scale bar in J represents 5 μm (A–F), 3.7 μm (G–L). Insets are 150% magnified.

(4.3 μm ± 0.4 SEM average length, n = 67; Figure 5A). Double-staining experiments revealed that patches of CLIP-190 were contained within dMyoVI-rich zones; the latter displayed a stronger tendency to spread into surrounding F-actin–containing areas (Figure 5A). CLIP-190 and dMyoVI patches closely surrounded MTs but clearly did not colocalize with them (Figure 5B). We also noted that dMyoVI labeled structures particularly in the cell body, which appeared to represent vesicles, and that low levels of CLIP-190 tended to colocalize at these structures (Supplemental Figure S3A). To assess functional interactions between dMyoVI and CLIP-190, we used loss-of-function mutant alleles of dMyoVI (*jar*^{322}/*Df(3L)Crb87-5*), which had previously been shown to remove all dMyoVI transcripts and protein (Morrison and Miller, 2008). Of importance, only 8.2% (n = 85) of neurons carrying these alleles displayed CLIP-190 patches in GCs (Figure 5C), and only small puncta remained along MTs and in the F-actin–rich periphery, which did not display the typical elongated shape of comets. Although these small puncta were similarly visible in wild-type control neurons (Figure 5C), these neurons clearly differed in the presence of prominent GC patches (89.9% of neurons; n = 69), strongly indicating that patch formation depends on the presence of dMyoVI.

Myosin-VI is a known minus end–directed motor, which accumulates at pointed (minus) ends of actin filaments (Cramer, 2000). Because pointed ends of actin filaments tend to localize away from the GC periphery, we speculated that F-actin is required for the patch localization of dMyoVI and consequently also of CLIP-190. In agreement with this hypothesis, we found that treatment with the actin-depolymerizing drug cytochalasin D causes severe loss of F-actin, as well as of dMyoVI and CLIP-190 patches in GCs. Similar to our observations with *jar* mutant neurons, only small puncta of CLIP-190 remained in cytochalasin D–treated neurons (Figure 5, E and F), and they were similarly observed with GFP::CLIP-190, for which live imaging revealed them to be relatively immobile spots that were not comets (Supplemental Movie S2). To test whether the three proteins follow a linear genetic hierarchy during patch formation (e.g., actin anchors dMyoVI, which, in turn, tethers CLIP), we analyzed CLIP-190–deficient neurons (see later discussion). These neurons displayed normal actin distributions, but only 35% of them (n = 74) showed the prominent dMyoVI patch, in comparison to 82% (n = 66) in wild-type neurons; Figure 5D). In contrast, vesicle-like structures in neuronal cell bodies were still clearly stained with anti-dMyoVI in the *CLIP-190* mutant condition (Supplemental Figure S3, B and C). Therefore primarily the colocalization at GC patches seems to involve mutual functional dependence, with CLIP-190 being more dependent on dMyoVI than vice versa (see *Discussion*).

We next tested whether GC patch localization of CLIP-170 in mouse neurons (Figure 5I) occurs through similar mechanisms as in *Drosophila*. When staining mouse primary cortical neurons for myosin-VI, we found prominent patches in their GCs (72% of neurons, n = 36; Figure 5K). We then tested the dependence on F-actin and treated neurons with cytochalasin D. GC patches of both myosin-VI and CLIP-170 were mostly absent in these neurons (Figure 5, J and L). However, F-actin is known to display some resistance to cytochalasin D treatment in mouse cortical neurons (Sattler *et al.*, 2000). Accordingly, we found that small, condensed patches of F-actin tended to remain in some GCs and that CLIP-170 and myosin-VI colocalized in these patches with statistically strong correlation (Pearson r = 0.57, n = 74; Figure 5J). Of note, just as observed in fly neurons, the absence of endogenous CLIP-170 from GC patches in mouse cortical neurons did not noticeably increase CLIP-170's MT plus end localization.

In conclusion, both CLIP-170 and CLIP-190 colocalize with type VI myosins into GC patches, dependent upon F-actin, and our data in *Drosophila* neurons indicate mutual stabilization of CLIPs and myosins in these patches (see *Discussion*). Absence of CLIP-190 GC patches never correlated with enhanced MT plus end localization, suggesting that MT plus ends do not compete for a limited pool of protein. Instead, down-regulation of MT plus end localization seems to depend on other, parallel mechanisms.

Distinct functional domains of CLIP-190 regulate patch localization and MT plus end tracking

We then carried out structure–function analyses to understand how the known functional regions of CLIP-190 contribute to the observed localization properties. CLIP-170 and CLIP-190 are composed of three regions (Figure 6A): the N-terminal head (H) region, which harbors the two CAP-Gly domains responsible for EB1 binding at MT plus ends; the central coiled-coil (CC) domain, which binds CLASP in mammals; and the C-terminal (C) region (containing two zinc knuckles and an ETY/F motif), which mediates kinetochore localization of CLIP-190 in *Drosophila* S2 cells, displays autoinhibitory functions, and binds to Lis1 and $p150^{glued}$ in CLIP-170 (Coquelle *et al.*, 2002; Goodson *et al.*, 2003; Dzhindzhev *et al.*, 2005; Weisbrich *et al.*, 2007; Gupta *et al.*, 2010).

To determine which domains are required for CLIP localization, we expressed GFP-tagged full-length and deletion constructs of both fly CLIP-190 and mammalian CLIP-170 in *Drosophila* neurons and studied their localization (Figure 6 and Supplemental Movie S3). To generate transgenic fly lines with standardized construct expression strength, we inserted Gal4-inducible versions of these constructs into the same genomic locus, respectively (see *Materials and Methods*).

We found that GFP::CLIP-170 displays robust patch localization in GCs of *Drosophila* neurons comparable to CLIP-190 (Figure 6, C and D), providing further confirmation that patch localization is a conserved feature. The two deletion constructs GFP::CLIP-190-CC-C (containing CC and C) and GFP::CLIP-190-CC (containing only CC) showed localization to GC patches comparable to endogenous CLIP-190, GFP::CLIP-190, or GFP::CLIP-170 (Figure 6, E and F). To test whether the localization of CC results from its specific ability to interact with dMyoVI, we tested whether dMyoVI coprecipitated with the CC fragment, H, or C regions. We found that dMyoVI coprecipitates only with CC (Figure 6B and Supplemental Figure S4). This clearly implicates the CC region as the region with which dMyoVI can interact to mediate GC patch localization of CLIP-190, further supporting our model that this localization is primarily actin based. In further agreement, we found that CLIP-190's patch localization was unchanged when splayed MTs we removed from GCs via treatment with the MT-destabilizing drug nocodazole (Figure 5, G and H).

Besides conserved patch localization, we observed that GFP::CLIP-170 in fly neurons deviates from GFP::CLIP-190 by showing some MT plus end tracking, comparable to findings with this construct in mouse neurons (Figures 3, B and D, and 6, C and D). To understand this deviation, we compared the localization of GFP::CLIP-190-H and an analogous GFP::CLIP-170-H construct (containing the H regions only) and found that both displayed reliable MT plus end tracking throughout neurons. However, the tracking was faint for GFP::CLIP-190-H and more prominent for GFP::CLIP-170-H (Figure 6, G and H). We therefore generated a hybrid construct in which the H regions were swapped (GFP::CLIP-170H-190CC-190C). In comparison to GFP::CLIP-190, this hybrid construct showed more reliable plus end tracking and a highly significant increase in comet intensity (Figure 6, C and I), suggesting that the head regions are essential mediators of this differential behavior. Taken together, these data indicate that H domains themselves display less affinity for MT plus ends in neurons than in nonneuronal contexts. On the other hand, the two H regions display comets in neurons far more reliably than the CLIP-190 full-length construct, suggesting that other functional domains of CLIPs might negatively interfere with MT plus end localization.

The C region of CLIP-170 has been shown in nonneuronal contexts to mediate autoinhibition by looping back and binding the H region (Lansbergen *et al.*, 2004). This might explain why most GFP::CLIP-190–expressing neurons show no comets (Figure 6C). To test this possibility, we expressed GFP::CLIP-190-H-CC (in which the C region is specifically deleted) and found reliable MT plus end tracking of a comparable strength to GFP::CLIP-190-H alone (Figure 6, G and L, and Supplemental Figure S5A). This finding is consistent with an inhibitory role of the C region in MT plus end localization and mirrors very similar effects reported for mammalian neurons transfected with either CLIP-170 or CLIP-170-H-CC (Stepanova *et al.*, 2003). This mechanism seems less prominent for GFP::CLIP-170 in *Drosophila* neurons (compare Figure 6, D vs. H), which may be due partly to the stronger affinity of its H domain for EB1 and partly to incompatibility of its autoinhibitory regulation with the signaling environment of *Drosophila* neurons.

To test whether inhibition through the C region can act in-*cis* or -*trans*, we coexpressed GFP::CLIP-190-C (consisting of only C) together with GFP::CLIP-190-H-CC in the same neurons, but comet formation was the same as in neurons expressing GFP::CLIP-190-H-CC alone (Supplemental Figure S5 and Supplemental Movie S4). This suggests that inhibition through the C region acts through an intramolecular mode, potentially conserved with the autoinhibitory mechanism in CLIP-170 (Lansbergen *et al.*, 2004; Mishima *et al.*, 2007). Of interest, single expression of GFP::CLIP-190-C or the comparable GFP::CLIP-170-ΔCC-C (containing a short segment of CC together with C; Neukirchen and Bradke, 2011) revealed no patterned distributions (Figure 6, J and K), and therefore they are unlikely to mediate CLIP localization in fly neurons. This is in further contrast to nonneuronal cells, in which the C region of CLIP-170 is recruited to sites of Lis1 and dynactin 1 localization (Coquelle *et al.*, 2002).

Taken together, our data suggest that patch and MT plus end localizations of CLIPs are independently regulated, in agreement with our conclusions from the F-actin or dMyoVI depletion experiments (see earlier discussion; Figure 5). In this scenario, the CC region regulates patch localization, whereas the H and C regions are responsible for the low degree of MT plus end localization.

Loss of CLIP-190 does not affect axon growth and function

We next tested whether the atypical localization of CLIP functionally contributes to axon growth. For this, we used our recently generated complete loss-of-function mutant allele (*CLIP-190^{KO}*; Figure 7; Dix *et al.*, 2013) and assessed it in homozygosis or over the small deficiency we generated (*Df(2L)CLIP-190*), which uncovers the CLIP-190 locus (Figure 7A). Although these mutant constellations abolished CLIP-190 immunoreactivity in cultured neurons or embryos (Figure 7, B and D) and in Western blots loaded with protein extracts from homozygous mutant flies (unpublished data), they gave rise to viable and fertile homozygous mutant flies. This provided us with the opportunity to remove the gene product from the germline, thus ensuring total loss of gene function from the earliest stages of development.

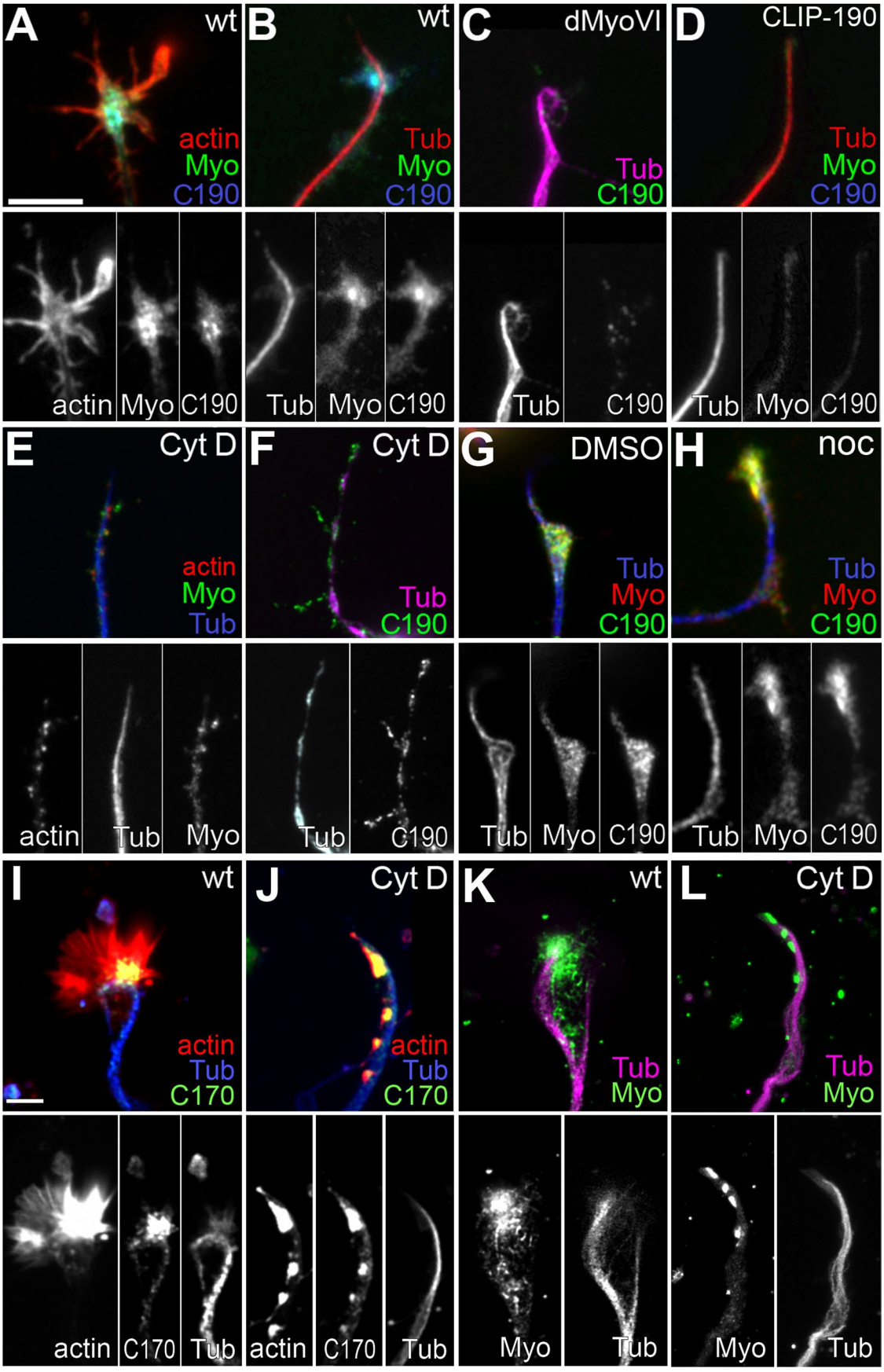

FIGURE 5: CLIP-190 requires dMyoVI and F-actin for patch localization. Images show *Drosophila* primary neurons at 6 h in culture that are untreated, treated with vehicle (DMSO), or treated with cytochalasin D (CytoD), derived from wt or

Using these mutant alleles, we analyzed axonal morphology in vivo and in culture using a number of different readouts. First, the length of motor nerves in embryos at stage 16 is a good readout for dysfunction of the axon growth machinery (Bottenberg *et al.*, 2009), but our length measurements showed no change in *CLIP-190^{KO}/Df(2L)CLIP-190* mutant embryos (103% ± 4.3 SEM normalized to wild type [wt]; $n = 74/10$, $p_{MW} = 0.77$; Figure 7E). Second, the midline of the embryonic CNS is an often used and very sensitive indicator of axonal growth aberration (Sánchez-Soriano *et al.*, 2007), but no defects were observed in CLIP-190–deficient embryos (Figure 7F). Third, anatomical changes of late larval neuromuscular junctions provide sensitive readouts for axonal morphogenesis (Prokop and Meinertzhagen, 2006). However, detailed analyses of neuromuscular junctions on ventral longitudinal muscles 3 and 4 (Landgraf *et al.*, 2003) of *CLIP-190^{KO}/Df(2L)CLIP-190* larvae revealed no obvious changes in the general morphology and no changes in overall terminal length (46% ± 2.4 SEM relative length in mutants compared with 45% ± 2.4 SEM in wt; $n = 24$, $p_{MW} = 0.798$; Figure 7G). Fourth, length and MT organization of the axons of cultured primary *Drosophila* neurons are arguably the most sensitive indicators for axonal growth machinery defects (Sánchez-Soriano *et al.*, 2010). However, primary neurons generated from embryos carrying various *CLIP-190* mutant constellations revealed no phenotypes (Figure 7, H and I). We also tested the effect of expressing the dominant-negative construct GFP::CLIP-170-ΔCC-C (Komarova *et al.*, 2002; Lansbergen *et al.*, 2004; Neukirchen and Bradke, 2011) and the analogous *Drosophila* construct GFP::CLIP-190-CC-C (Figure 6), but they caused no measurable phenotypes in *Drosophila* primary neurons (Figure 7I).

Finally, we turned to potential intracellular phenotypes using EB1::GFP and LysoTracker as readouts. First, it has been suggested that CLIPs can influence MT polymerization dynamics in axons (Stepanova *et al.*, 2010; Neukirchen and Bradke, 2011). Therefore we measured the velocity and lifetime of EB1::GFP in wt and *CLIP-190* mutant neurons. Consistent with our axon growth data, there were no measurable changes between the two neuron groups (Supplemental Figure S6). Second, it was recently shown that CLIP-170 can function in GCs to initiate dynein/dynactin-based retrograde transport of late endosomes along axonal MTs (Moughamian *et al.*, 2013) and that loss of dMyoVI increases the mobility of synaptic vesicles at the *Drosophila* neuromuscular junction (Kisiel *et al.*, 2014). The GC patches of CLIPs and type VI myosins are candidate execution sites for regulating local trafficking since they are situated precisely where transfer between actin-based local and MT-based long-range transport occurs (Kapitein *et al.*, 2013). To test this possibility, we performed live imaging on wt and *CLIP-190* mutant neurons, both stained with the fluorescent LysoTracker dye, which labels the late endosomal/lysosomal compartment (Lewis and Lentz, 1998). We measured the velocity of LysoTracker-labeled vesicles in the GC and the axon, as well as the overall direction of vesicle movement over a 4-min period per neuron (Supplemental Figure S6). Although *CLIP-190* mutant neurons showed a tendency toward faster vesicle motion in axons and a very slight bias toward retrograde movement, these data do not suggest a prominent role of the CLIP-190/dMyoVI complex in initiating retrograde lysosome transport in *Drosophila* neurons.

Thus none of our analyses indicated any obvious role for CLIP-190 in developing fly neurons. In contrast, neurons lacking dMyoVI (*jar^{322}/Df(3L)Crb87-5*) displayed reduced axon growth down to ~80% of wt control neurons, combined with a strong increase in noncoalescence of MTs in GCs (Supplemental Figure S7). Because these phenotypes are not seen upon loss of CLIP-190, we consider them the result of dMyoVI functions independent of CLIP-190.

CLIP-190 shows no detectable functional overlap with other +TIPs

As one last possibility, we reasoned that potential functions of CLIP-190 in axons might be masked by the functions of other +TIPs. To test this possibility, we assessed the *CLIP-190^{KO}* allele in double- and triple-mutant constellations using the same mutant alleles of other neuronal +TIPs as in our CLIP-190 localization studies (Figure 4, G and L). For these experiments, we used primary neurons, which provide more sensitive readouts for cytoskeletal studies than in vivo analyses (Sánchez-Soriano *et al.*, 2010). First, we assessed whether the +TIP mutant alleles alone caused axonal growth phenotypes. We found that loss of dCLASP (*chb^{2}*, homozygous or over deficiency *Df(3L)BSC553*) and loss of Shot (*shot^{3}*) both caused axon shortening, consistent with findings in vertebrate/mammalian neurons (Sánchez-Soriano *et al.*, 2009; Hur *et al.*, 2011; Marx *et al.*, 2013). In contrast, the *Apc2^{g10} Apc^{Q8}* double mutation or loss of the dynein/dynactin- complex member Glued (*Gl^{Δ22}*) or dynein heavy chain 64C (*dhc64C$^{4-19}$*; Prokop, 2013) caused axon lengthening (Figure 7), opposite to previous findings in mice, rats, or chicks (Zhou *et al.*, 2004; He *et al.*, 2005; Ahmad *et al.*, 2006; Grabham *et al.*, 2007; Abe *et al.*, 2008; Lazarus *et al.*, 2013). These opposing phenotypes might be due to deviations in the culture conditions under which our fly neurons are grown or a consequence of the qualitatively different readouts provided by the far shorter fly axons.

We then combined these mutant alleles into double- or triple-mutant combinations with *CLIP-190^{KO}* and analyzed them in *Drosophila* primary neurons. These studies revealed that the mutant phenotypes of *chb^{2}*, *Apc^{Q8} Apc2^{g10}*, Gl^{Δ22}, and *shot^{3}* were completely unaffected by additional loss of CLIP-190 (Figure 7I). Therefore axon growth seems not to depend on overlapping functions

jar^{322}/Df(3L)Crb87-5 mutant embryos (dMyo), and stained for tubulin (Tub), F-actin (actin), endogenous dMyoVI (Myo), and/or endogenous CLIP-190 (C190), all as indicated. (A) Endogenous dMyoVI and CLIP-190 localize to patches in the center of the actin-rich GC. (B) dMyoVI and CLIP-190 patches are not closely colocalized to MTs. (C) In neurons deficient for dMyoVI, CLIP-190–stained patches in GCs are abolished. (D) In neurons deficient for CLIP-190, dMyoVI-stained patches are also absent. (E, F) In neurons treated for 4 h with 0.4 µg/ml cytochalasin D (an actin polymerization inhibitor), CLIP-190– and dMyoVI-stained patches in GCs are abolished. (G, H) Removing splayed MTs using nocodazole treatment (20 µM for 2.5 h) does not disrupt formation of dMyoVI and CLIP-190 patches in comparison to DMSO-treated control neurons. (I) In cultured mouse cortical neurons, DMSO-treated control cells display localization of endogenous CLIP-170 to patches in GCs, which are in F-actin–rich regions (shown by phalloidin costaining). (J) On treatment with cytochalasin D, F-actin becomes localized to condensed patches, to which CLIP-170 generally colocalizes. (K, L) Cytochalasin D treatment causes redistribution of endogenous myosin-VI from the single broad patch in the GC seen in control DMSO-treated cells (K) to small, strong patches (L). This is comparable to the effect on CLIP-170. Scale bar in A represents 5 µm (A–H), 10 µm (I–L).

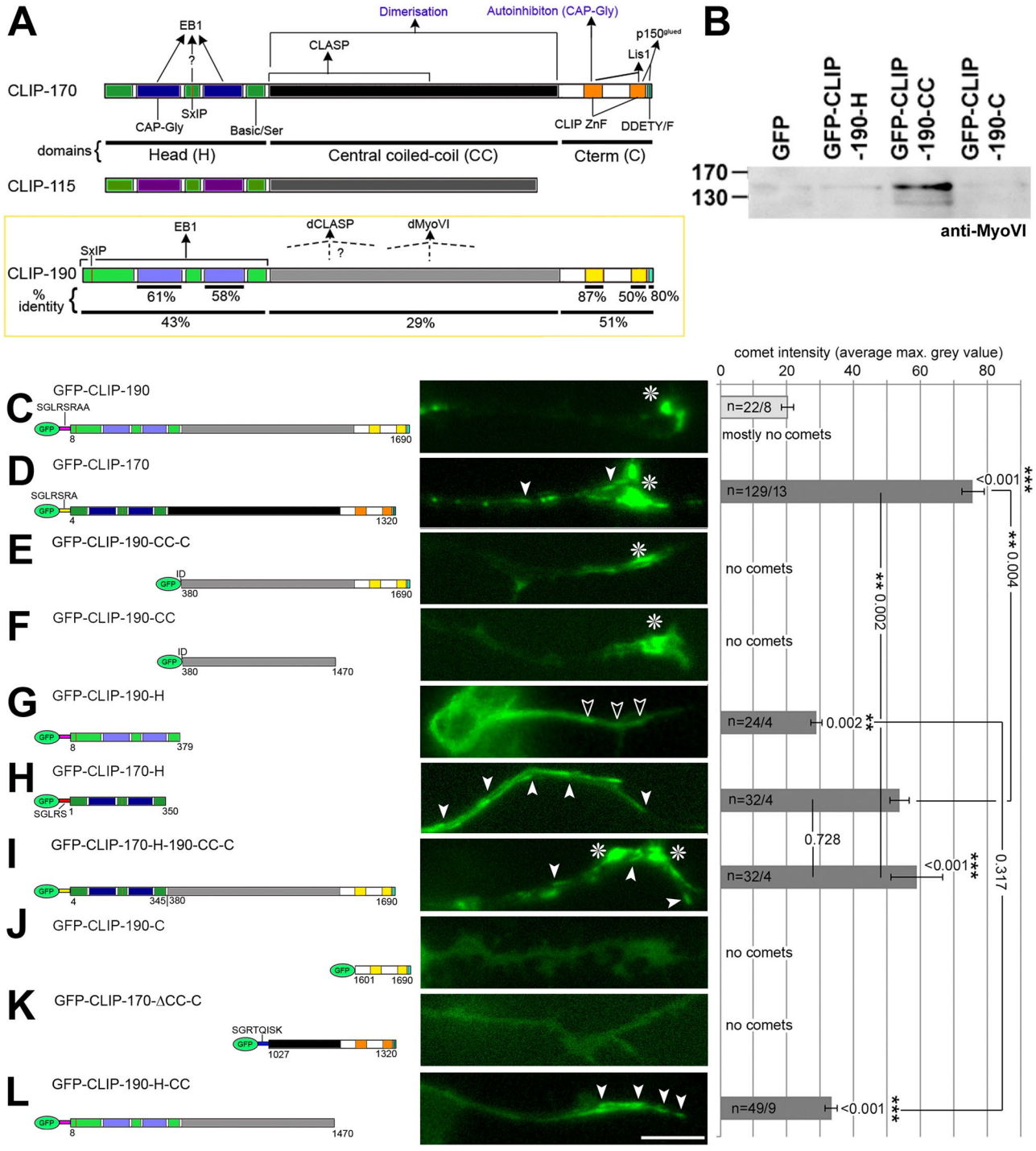

FIGURE 6: Domain requirements for neuronal localization of CLIPs in *Drosophila* neurons. (A) Mammalian CLIP-170 and -115 and *Drosophila* CLIP-190 contain the same functional domains and motifs (mammalian/fly): serine-rich regions of H region (dark/light green), SxIP motifs (red/red), CAP-Gly domains (dark/light blue), coiled-coil domain (black/gray), zinc knuckle motifs (orange/yellow); and DDETY/F motif (dark/light turquoise). Reported interaction partners of CLIP-170 and CLIP-190 are indicated by arrows (see the text for details). Percentages of amino acid sequence identity between CLIP-190 and CLIP-170 are indicated below CLIP-190. (B) GFP-trap from S2 cell extracts expressing GFP (control) or GFP-tagged CLIP-190-H, -CC, or –C, as indicated, here immunoblotted with anti-dMyoVI. Molecular weight (kilodaltons) is indicated on the left. Specific coprecipitation of dMyoVI was only seen with the CC fragment (see Supplemental Figure S4 for more information). (C–L) Left, GFP-tagged transgenic UAS-constructs of CLIP-170 and CLIP-190 (as indicated; colors are the same as in A); middle, still images from live movies of *Drosophila* primary neurons at 6 h in culture expressing the respective constructs (asterisks, immobile patches; open arrowheads, faint MT plus end trailing comets; filled arrowheads, prominent comets). Scale bar in K represents 5 μm in all images. Right, quantification of the strength of comet localizations of the GFP-tagged transgenic UAS-constructs of CLIP-170 and CLIP-190, as shown in C–L; note that measurements in B were taken from the few neurons displaying visible comets (therefore bar shown in light gray). Using

between CLIP-190 and the other +TIP factors, and roles of CLIP-190 in nervous system formation appear negligible or subtle at most.

DISCUSSION

CLIP-170 and CLIP-190 do not show prominent MT plus end tracking in neurons

The polymerization, targeting, and stability of MTs are believed to be essential in regulating axon growth and path finding, as are the +TIPs as the likely regulators of these processes (Chilton and Gordon-Weeks, 2007; Akhmanova and Steinmetz, 2008; Conde and Caceres, 2009; Prokop *et al.*, 2013). CLIP-170 has been widely studied in interphase cells, where its prominent plus end tracking is believed to promote MT rescue and polymerization (Rickard and Kreis, 1990; Perez *et al.*, 1999; Komarova *et al.*, 2002; Arnal *et al.*, 2004; Gupta *et al.*, 2009; Nakano *et al.*, 2010). It was therefore unexpected that *Drosophila* CLIP-190 and its close mammalian homologue CLIP-170 are not prominent tip trackers in growing axons, which contain highly dynamic MTs (Stepanova *et al.*, 2003). These findings highlight an unexpected degree of cell-specific regulation and likely explain the lack of CLIP-190 functions in developing axons in vivo and in culture.

We find that in fly and mammalian neurons, CLIP-170 and CLIP-190 localize to patches in GCs and that, even when overexpressed in neurons, their +TIP tracking is far less prominent than in nonneuronal cells. Other mammalian reports do not contradict what we observed. Previous studies used CLIP-170/115 localization in combination because CLIP-170 antibody staining alone failed to reveal MT comets (Stepanova *et al.*, 2003; Neukirchen and Bradke, 2011). GFP::CLIP-170 has been used successfully as a plus end marker in cultured CNS neurons of *Xenopus laevis* (Lee *et al.*, 2004), consistent with our observations in fly and mouse neurons (Figures 3 and 6), but it has also been reported to form aggregates in neurons (Stepanova *et al.*, 2003). Those aggregates were interpreted as overexpression artifacts, whereas we suggest that they represent genuine actin- and myosin-VI–dependent patch localization. In terms of neuronal MT dynamics, our results demonstrate that complete CLIP-190 deficiency has no significant effect, which might similarly be true for CLIP-170 in mammalian neurons, although reports are inconsistent (Stepanova *et al.*, 2010; Neukirchen and Bradke, 2011; Moughamian *et al.*, 2013). On balance, there is no strong support for a major role for CLIP-170 during axon growth. Regarding axon growth, promoting roles of CLIPs were suggested from studies with combined loss of CLIP-170 and CLIP-115. Of these, CLIP-115 is more strongly expressed in neurons, it is unlikely to display autoinhibition of MT plus end localization since it lacks the C domain (Figure 6A; De Zeeuw *et al.*, 1997), and it is the only CLIP linked to a brain disorder (Williams–Beuren syndrome; OMIM #194050). Therefore CLIP-115 is arguably the better candidate to act as a MT regulator and growth-promoting factor in axons. Its roles may represent an evolutionary adaptation required in larger animals with long axons, and CLIP-170 might not share this role.

Why do CLIPs behave differently in neurons?

CLIP-170 and CLIP-190 display considerably less MT plus end localization in neurons than in nonneuronal cells. Our experiments clearly showed that this is not due to protein depletion induced by CLIP recruitment to prominent GC patches. Instead, our H-CC and H domain deletion constructs suggested autoinhibition through the C region as one mechanism, similarly described for CLIP-170 in nonneuronal cells (Lansbergen *et al.*, 2004; Mishima *et al.*, 2007; Lee *et al.*, 2010). Because autoinhibition of CLIP-170 is regulated by phosphorylation of its H domain likely through protein kinase A (Lee *et al.*, 2010), differences in kinase activities in neurons versus nonneuronal cells could explain the context-specific behaviors of CLIPs. In parallel, the H domain displays an inherently low association with MT plus ends, and this could be caused by 1) the very different nature of MT networks in axons and/or 2) their distinct intracellular signaling environments. First, axonal MTs are decorated by MT-stabilizing proteins, including MAP1B, tau, and spectraplakins, and all of these proteins have been demonstrated to influence MT polymerization (Feinstein and Wilson, 2005; Alves-Silva *et al.*, 2012; Tymanskyj *et al.*, 2012; Tortosa *et al.*, 2013). Here we showed that the spectraplakin Short stop does not affect CLIP-190 localization (Figure 4J), but MAP1B and tau might well display such influences. Second, the intracellular signaling milieu of neurons might determine low plus end localization. A precedent for such regulation is provided by the AMP-activated protein kinase in nonneuronal cells, which increases MT plus end affinity of CLIP-170 through phosphorylation of its H domain (Nakano *et al.*, 2010). This possibility was not tested here.

CLIP-170 and CLIP-190 display atypical patch localization in neuronal GCs. For CLIP-190, we clearly showed that patch localization is not a cell culture artifact but occurs similarly in vivo. We could induce similar patches through CLIP-190 overexpression in leading edge cells of the epidermis during dorsal closure (Figure 1F). Like growth cones, these epidermal cells display prominent lamellipodia and prominent accumulations of dMyoVI (Lin *et al.*, 2007). CLIP-190 patches in GCs might therefore be the outcome of existing dMyoVI accumulation combined with available CLIP protein pool due to low affinity for MT plus ends. In this scenario, myosin-VI accumulates in F-actin–rich lamellipodia of GCs, where it coassembles with CLIP-190 through direct interaction with its CC domain (Figure 6). This complex then seems to become activated to migrate toward minus ends of F-actin and accumulate into patches within GCs, as suggested by the partially reciprocal dependence of myosin-VI and CLIP-190 during complex formation. This activation of myosin-VI processivity may involve its dimerization induced by binding to cargo proteins, as described for optineurin transport (Phichith *et al.*, 2009). In this example, myosin-VI binds the coiled-coil region of optineurin (Sahlender *et al.*, 2005), and this region aligns with the CC region of both CLIP-170 and CLIP-190 (24% identity; unpublished data). This same CC region was pinpointed by our structure–function analysis and binding assays to mediate CLIP-190's interaction with dMyoVI and GC patch location (Figure 6, B and F), thus adding further support to a sequence of events that can explain this prominent localization of both proteins and is consistent with all of our data and the literature.

Conclusions

Our results for CLIP-170 and CLIP-190 clearly demonstrate that roles of MT regulators understood from nonneuronal cells do not necessarily apply in neurons and should be reevaluated before

imaging with identical settings, mean comet intensity was calculated from the maximum gray value of comets (after background subtraction). p_{MW} values were determined following ANOVA, which indicated a highly significant difference in intensity between groups (***$p < 0.001$). The p_{MW} values relative to GFP::CLIP-190 are given above the bars, and other comparisons are given as indicated; sample numbers (n) and SEM (error bars) are also indicated.

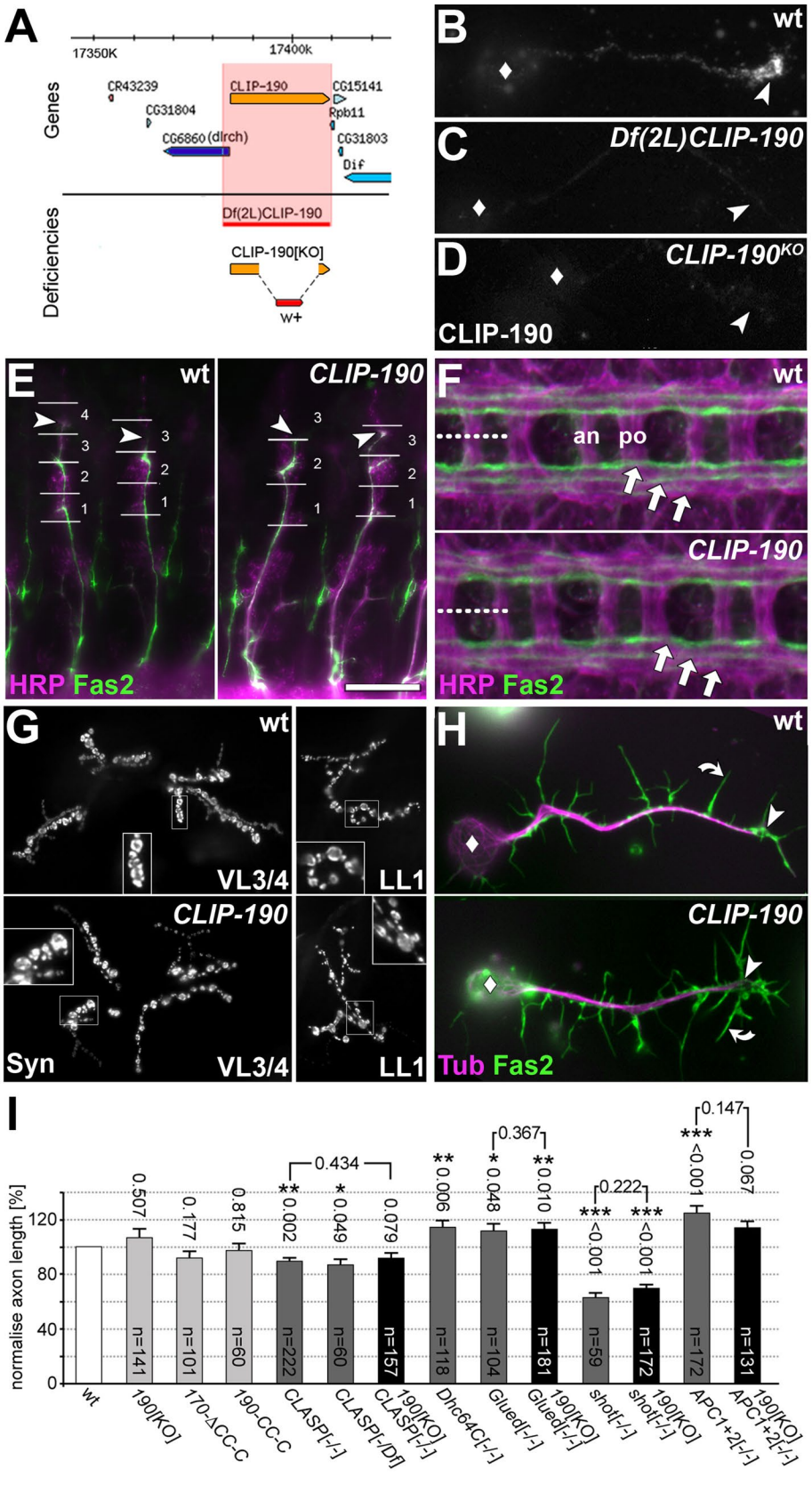

FIGURE 7: CLIP-190 loss of function does not affect axon growth. All images compare wt with *CLIP-190*^{KO} mutant neurons, unless stated otherwise. (A) Genomic region of chromosome 2L containing the *CLIP-190* gene (modified from the GBrowse view on FlyBase); the red-shaded area shows the genomic region deleted in *Df(2L)CLIP-190* (based on P-element locations); as indicated below, *CLIP-190*^{KO} is a deletion within the CLIP-190 locus, replaced by the *mini-white* gene (w^{+}; Dix *et al.*, 2013). *Drosophila* primary neurons at 6 h in culture, derived from embryos that were (B) wt or homozygous for either (C) *Df(2L)CLIP-190* or (D) *CLIP-190*^{KO} (diamonds indicate cell bodies, arrows indicate GCs); no obvious staining for CLIP-190 can be detected in both cases; the maternal contribution of CLIP-190 was removed by using homozygous mutant mothers. (E) Fas2-stained motor nerves (green) in stage 16 embryos (anterior left, dorsal up) costained for the neuronal surface marker HRP (magenta), which labels sensory neurons (asterisks) as landmarks for nerve measurements (white reference lines according to Bottenberg *et al.*, 2009); arrowheads indicate dorsal tips of motor nerves. (F) CNS of stage 16 embryos stained for HRP (magenta) and Fas2 (green); Fas2 stains three parallel longitudinal axon tracts (white arrows) on each side of the midline (indicated by stippled line), but no staining is seen in the anterior (an) and posterior (po) commissures. (G) Late larval neuromuscular junctions on muscles VL3/4 and LL1 (as indicated; nomenclature according to Bate, 1993) stained for the presynaptic marker synapsin; boxed areas show boutons, which are shown as 2× magnified insets. (H) Embryo-derived *Drosophila* primary neurons after 6 h in culture stained for tubulin (magenta) and F-actin (green); soma (so), axon tips (arrowheads), and filopodia (curved arrows) are indicated. (I) Quantification of axon length measurements of primary neurons with distinct genotypes as indicated in the graph; p_{MW} values relative to wt are given above each bar and single comparisons at the top; sample numbers (*n*) and SEM (error bars) are indicated; gray bars show single-mutant conditions (from left to right: *CLIP-190*$^{KO/KO}$, *sca-Gal4 UAS-GFP-CLIP-170-ΔCC-C*, *sca-Gal4 UAS-GFP-CLIP-CC-C*, *dCLASP*$^{2/2}$, *dCLASP*$^{2/Df(3L)BSC553}$, *dhc64C*$^{4\text{-}19/4\text{-}19}$, *Gl*$^{\Delta 22/\Delta 22}$, *shot*$^{3/3}$, *APC2*$^{g10/g10}$, *APC1*$^{Q8/Q8}$); black bars show double- or triple-mutant conditions of *CLIP-190*$^{KO/KO}$ with other mutant alleles. Scale bar in E represents 5 µm (B–D), 35 µm (E), 20 µm (F), 50 µm (G), 10 µm (H).

including them in models of neuronal cell biology. The observed differences are helpful in readjusting our views on what are the most promising candidate proteins for future research in neurons and also in rethinking the roles of CLIPs in nonneuronal cells. For example, besides actin-dependent accumulations reported here, prominent stable accumulations of CLIPs have been reported in other contexts. Thus CLIP-170 and CLIP-190 localize to kinetochores in a dynein/dynactin- and Lis1-dependent manner (Coquelle *et al.*, 2002; Dzhindzhev *et al.*, 2005), and CLIP-170 was shown to stably localize and function at the spermatid manchette (Akhmanova *et al.*, 2005). Generally,

functional roles of CLIPs have remained elusive, and the finding that complete loss of CLIP proteins in mammals or *Drosophila* is not lethal (Miedema, 2007; Dix *et al.*, 2013; our findings) suggests that their functions are subtle. Therefore future investigations might have to focus more on the emerging atypical modes of CLIP localization, including links to actin-binding proteins such as myosin-IV, for which potential roles have already been proposed in the context of intracellular trafficking, both in mammals (Hasson, 2003; Buss and Kendrick-Jones, 2008) and in *Drosophila* (Finan *et al.*, 2011). For example, the actin-binding Golgi protein Lava lamp binds both dMyoVI and CLIP-190 in nonneuronal cells (Sisson *et al.*, 2000; Papoulas *et al.*, 2005; Finan *et al.*, 2011), and mammalian CLIP-170 has been suggested to link MTs to endocytic vesicles and melanosomes, structures at which myosin- VI is also known to localize (Pierre *et al.*, 1992; Lomakin *et al.*, 2009; Loubery *et al.*, 2012).

MATERIALS AND METHODS

Fly strains

Oregon R wild-type strain and the following mutant fly stocks were used: for *CLIP-190*, the *Df(2L)CLIP-190*, *pUb-Rpb11-2* fly strains (explained later), a larger deficiency (*Df(2L)BSC294*), and the *CLIP-190^{KO}*-null mutant allele (Dix *et al.*, 2013); for *dMyoVI*, the null mutant allele *jaguar^{322}* (*jar^{322}*) in combination with deficiency *Df(3L)Crb87-5* (a constellation completely abolishing dMyoVI function; Morrison and Miller, 2008); for *dCLASP*, the amorph allele *chromosome bows 2* (*chb^{2}*; Inoue *et al.*, 2000) in homozygosis or over deficiency *Df(3L)BSC553*; for *p150^{Glued}*, the null mutant allele *Glued$^{\Delta 22}$* (*Gl$^{\Delta 22}$*; removing 3.2 kb of the transcription unit including the presumptive start site; Siller *et al.*, 2005) either in homozygosis or over deficiency *Df(3L)BSC737*; for *Lis-1*, the P-element insertion *lis1^{K13209}* (Swan *et al.*, 1999; reducing Lis-1 protein to near-undetectable levels in second-instar larvae when in heteroallelic constellation with *Lis1$^{G10.14}$*; Siller *et al.*, 2005); for *Dhc*, the null mutant allele *dhc64C$^{4-19}$* (Gepner *et al.*, 1996); for *short stop*, the null mutant allele *shot^{3}* (Kolodziej *et al.*, 1995); and for APCs, the null mutant allele *APC^{Q8}* (glutamine 426 converted to Stop codon) and the amorphic allele *APC2^{g10}* (Ahmed *et al.*, 1998; Akong *et al.*, 2002; McCartney *et al.*, 2006). To allow selection of homozygously mutant embryos, mutant alleles were kept over second and third chromosomal balancers harboring *twist-Gal4*, *UAS-GFP* (Halfon *et al.*, 2002). Most lines carrying *UAS-* or *hs*-linked constructs of *CLIP-170* and *CLIP-190* were generated by us (see later description); other transgenic lines were as follows: *UAS-N-CLIP-170-GFP* (from Tom Millard, The University of Manchester, UK; Stramer *et al.*, 2010), *UAS-dCLASP* (from D. van Vactor, Harvard University; Lee *et al.*, 2004), *UAS-dMyoVI* (from K. Miller, University of Washington; Noguchi *et al.*, 2006), *UAS-Apc* (from M. Peifer, University of North Carolina, Chapel Hill; Roberts *et al.*, 2012), *UAS-EB1* (from P. Kolodziej, Vanderbilt University; Alves-Silva *et al.*, 2012), the driver line *scabrous-Gal4* (*sca-Gal4*) for targeted expression of UAS constructs in cultured neurons (Sánchez-Soriano *et al.*, 2010), *elav-Gal4* for the expression in the nervous system of the stage 16 embryo (Luo *et al.*, 1994), and *serpent-Gal4* (*srp-GAL4*) recombined with *UAS-mCherry-Moesin* for hemocyte analyses in vivo (Stramer *et al.*, 2010).

Generation of *Df(2L)CLIP-190*

The small deficiency *Df(2L)CLIP-190* uncovers the entire CLIP-190 gene and was generated with the flippase recognition target (FRT) method (the DrosDel method; Venken and Bellen, 2007) using two FRT site-bearing transposable elements inserted at the *CLIP-190* locus, that is, the P-element insertion *UM-8081-3* (DrosDel) and the RB piggyBac insertion *e02028* (Harvard Exelixis Collection; drosophila.med.harvard.edu/). *Df(2L)CLIP-190* in homozygosis caused loss of CLIP-190 protein, as confirmed by Western blot from flies and immunostaining in cultured neurons (Figure 7), but it was homozygous lethal due to a small C-terminal truncation of the adjacent Rpb11 gene. Introduction of the *pUb-Rpb11-2* rescue construct into *Df(2L)CLIP-190* background gave rise to viable fly stocks, and the stock *Df(2L)CLIP-190, pUb-Rpb11-2* was used in this study. To generate *pUb-Rpb11-2*, the genomic region of Rpb11 was amplified by PCR (using High Fidelity polymerase EXL; Agilent Technologies, Santa Clara, CA) and cloned in the correct orientation into the *Not*I site of the pWR-PUbq transformation vector (kindly provided by Nick Brown, University of Cambridge, UK), and transgenic flies carrying a second chromosomal insertion were generated (Genetic Services, Cambridge, MA).

CLIP constructs

Cloning steps were carried out in modified *pcDNA3.1* vector (ampicillin resistant; Invitrogen; Alves-Silva *et al.*, 2012), and inserts were eventually transferred to *M-6-attB-UAS-1-3-4* (chloramphenicol-resistant vector; Alves-Silva *et al.*, 2012) using *Asc*I and *Pac*I restriction sites. *M-6-attB-UAS-1-3-4*–borne constructs were used to generate transgenic fly lines (outsourced to BestGene, Chino Hills, CA) via PhiC31-mediated site-specific insertion into chromosomal location 62E1 on 3L using the *PBac{y^{+}-attP-3B}^{VK00031}* line (Bloomington line #9748).

CLIP-190 constructs were sequenced using appropriate primers from within the *CLIP-190* gene, and GFP-seq.fw, GFP-seq2.fw, and shotseq4.fw (GFP) were used to sequence from within GFP (Supplemental Table S2). T7.fw and SP6.rev were used to sequence into each side of the multiple cloning site of pcDNA3.1, whereas M13.fw and M13.rev were used to sequence into the multiple cloning site of M-6-attB-UAS-1-3-4.

To generate *GFP-CLIP-190* flanked by *Not*I sites, the *CLIP-190* coding sequence from *LD05834* cDNA was cloned into the *pBlue-Script SK* vector (ampicillin resistant) using *Eco*RI and *Xho*I sites. The *Xho*I site was replaced with *Not*I by insertion of an adaptor containing a *Not*I site with *Xho*I-compatible sticky ends. An adaptor sequence containing *Age*I and *Xho*I sites was then introduced by insertion into the *Eco*47III site just after the start codon of *CLIP-190*. GFP from the *pEGFP-C1* vector (Clontech, Mountain View, CA) was inserted using these *Age*I and *Xho*I sites.

Using *Not*I digest, the *GFP-CLIP-190* insert was transferred to pcDNA3.1 (*pcDNA3.1-GFP-CLIP-190*; Supplemental Figure S1). To generate *GFP-CLIP-190-H-CC*, *Eco*RI digest was used to transfer a truncated version of the insert from *pBluescript-GFP-CLIP-190* into *pcDNA3.1*. To generate *GFP-CLIP-190-H*, *pcDNA3.1-GFP-CLIP-190* was PCR amplified with *NotI-GFP.fw* and *ApaI-Pac-CLIP-H.rev*, and *Not*I/*Apa*I digest was used to transfer the fragment into *pcDNA3.1*. To generate *GFP-CLIP-190-C*, *pcDNA3.1-GFP-CLIP-190* was PCR amplified 1) with *NotI-GFP.fw* and *CLIP-190-Cterm-GFP.rev* to amplify the enhanced GFP (EGFP) and 2) with *GFP-CLIP-190-Cterm.fw* and *XhoI-CLIP-190.rev* to amplify CLIP-190's C-terminal domain; the PCR products were run through a PCR cleanup kit, and 1 µl of each was added to a fresh PCR mix to allow the two products to anneal; this was run for five cycles before primers *Not*I-GFP.fw and *Xho*I-CLIP-190.rev were added and the PCR run until completion to amplify *GFP-CLIP-190-C* as a single PCR product. *Not*I/*Xho*I digest was used to insert the product into *pcDNA3.1*. To generate *GFP-CLIP-190-CC-C*, first a version of *pcDNA3.1* containing EGFP with a downstream *Cla*I restriction site was engineered (*pcDNA3.1-GFP-ClaI*). EGFP was PCR amplified from *pcDNA3.1-GFP-CLIP-190* using *Kpn*-GFP.fw and *Bam*HI-ClaI-GFP.rev primers, and the product and

pcDNA3.1 were both cut sequentially with *Kpn*I and then *Bam*HI enzymes in their ideal buffers (Roche, Penzberg, Germany), with a heat inactivation step in between (65°C for 15 min). The EGFP insert was then ligated into the cut vector using T4 DNA ligase (Roche). In all of the following cases in which plasmids were cut at the *Cla*I restriction site, they were first grown in a *dam* mutant strain (One Shot INV110 *Escherichia coli* [Invitrogen, Waltham, MA] or SCS110 [Agilent Technologies]). Then *pcDNA3.1-GFP-CLIP-190* was PCR amplified using *ClaI-deltaH.fw* and *Not1-deltaH.rev*, and *Not*I/*Cla*I digest was used to insert the fragment into *pcDNA3.1-GFP-ClaI*. To generate *GFP-CLIP-190-CC*, the *Kpn*I and *Eco*RI fragment of *pcDNA3.1-GFP-CLIP-190-CC-C* was ligated into *Kpn*I and *Eco*RI–digested pcDNA3.1.

Rat-derived *GFP-CLIP-170* (GenBank reference AJ237670; kindly provided by Anna Akhmanova (Utrecht University, Netherlands) as a *Xho*I/*Sal*I-flanked 192–4597 nucleotide coding sequence of CLIP-170 in pEGFP-C1; kanamycin resistant [Clontech]) was PCR amplified with *Asc*I-EGFP.fw and *Pac*I-CLIP170.rev, and *Asc*I/*Pac*I digest was used to transfer the insert directly into *M-6-attB-UAS-1-3-4*.

To generate *GFP-CLIP-170H-190CC-190C*, M-6-attB-UAS-1-3-4-GFP-CLIP-170 was PCR amplified using *Asc*I-EGFP.fw and *Cla*I-CLIP-170-H.rev, and *Asc*I/*Cla*I digest was used to transfer the fragment into *pcDNA3.1-GFP-CLIP-190-CC-C*.

GFP-CLIP-170-ΔCC-C (amino acids 1027–1320 of *AJ237670* in a kanamycin-resistant pEGFP-C1 vector [Clontech], kindly provided by Dorothee Neukirchen, Max Planck Institute, Martinsried, Germany) was originally generated by Anna Akhmanova (Mimori-Kiyosue *et al.*, 2005). The insert was PCR amplified with *Asc*I-EGFP.fw and *Pac*I-DNCLIP170.rev (Supplemental Table S2), and *Asc*I/*Pac*I digest was used to transfer the insert directly into *M-6-attB-UAS-1-3-4*.

To generate *Drosophila* S2 cell expression plasmids, the CLIP-190 H, CC, and C regions as before were PCR amplified from *pcDNA3.1-GFP-CLIP-190* and transferred to the *pENTR* vector using TOPO cloning kit (Life Technologies, Waltham, MA). The inserts were fully sequenced and, using Gateway LR clonase II (Life Technologies), were transferred into a destination vector containing N-terminal GFP tag and metallothionein promoter for $CuSO_4$-induced expression (*pMT-GW*).

Drosophila primary neuron cultures

To generate *Drosophila* primary neuron cultures, neurons were extracted from stage 11 embryos (Campos-Ortega and Hartenstein, 1997) of either sex. Two methods were used and yielded comparable results. Either cells were removed via pulled needles and micromanipulator and transferred to Schneider's medium with 20% fetal calf serum (Schneider's/FCS) as detailed elsewhere (Prokop *et al.*, 2012), or whole embryos were treated for 1 min with bleach to remove the chorion, sterilized for ~30 s in 70% ethanol, washed in sterile Schneider's/FCS, and eventually homogenized with micropestles in 1.2- to 2-ml tubes (Eppendorf, Hamburg, Germany) containing 21 embryos/100 µl of dispersion medium. A 200-ml amount of dispersion medium contained 30 ml of Hank's balanced salt solution (Life Technologies), 3 ml of penicillin/streptomycin solution (Life Technologies), 0.01 g of phenyl-thio urea (Sigma-Aldrich, St. Louis, MO), 167 ml of distilled water, 0.5 mg/ml collagenase (Worthington, Lakewood, NJ), and 2 mg of dispase (Roche). Cells harvested with either of the two methods were treated for 5 min at 37°C with dispersion medium, washed, and then resuspended in Schneider's/FCS (4.3 µl of medium/embryo used). Thirty-microliter drops were placed on coverslips and kept as hanging drop cultures in air-tight special culture chambers usually for 6 h at 26°C (Prokop *et al.*, 2012). Incubation with 0.4 µg/ml cytochalasin D (kept as 1020 µg/ml stock solution in dimethyl sulfoxide [DMSO] and prediluted in sterile H_2O) lasted between 10 min and 4 h as stated. Incubation with 20 µM nocodazole (kept as 10 mM stock solution in DMSO and prediluted in sterile H_2O) lasted 2.5 h (changed once with fresh nocodazole after 1.5 h).

Mammalian cell lines

NIH/3T3 fibroblasts were grown in DMEM4 with 1% glutamine (Invitrogen), 1% penicillin/streptomycin (Invitrogen), and 10% FCS in culture dishes (100 mm with vents; Fisher Scientific, Loughborough, UK) at 37°C in a humidified incubator at 5% CO_2. Cells were split every 2–3 d: old media were removed, washed with prewarmed phosphate-buffered saline (PBS), and incubated with 4 ml of trypsin-EDTA at 37°C for 5 min (tapping the culture dish to deadhere the cells); then 7 ml of fresh culture medium was added, and cells were fully suspended by pipetting them 10 times up and down and diluted (1/3 to 1/20 dilution) in a culture dish containing 10 ml of culture medium.

Mouse epithelial EpH4 cells were grown in 50% DMEM, 50% Ham's F-12, 5% FCS, 5 mg/ml insulin. and 1% penicillin/streptomycin. Splitting cells was carried out every 2-3 d as described for NIH/3T3 cells, but trypsin was added for 10 min (37°C) and dishes were tapped harder to deadhere cells. The reaction was stopped by addition of 7 ml of medium, and cells were pipetted up and down 30 times.

In both cases, to prepare cells for immunostaining, 300–1000 µl of trypsinized cells were added to each well in a six-well plate containing sterile glass coverslips and diluted with 2 ml of medium. These were then left overnight to adhere and grow before fixing.

For transfection of NIH/3T3 cells, 2 ml containing ~100 cells/ml was first transferred to six-well plates and grown overnight to double cell density. To prepare DNA/Lipofectamine for transfection, 2 µg of DNA (GFP-CLIP-170) and 2 µl of Plus reagent (Invitrogen) were added to 1 ml of medium (without serum) in a centrifuge tube and incubated for 5 min at room temperature. A 6-µl amount of Lipofectamine (Invitrogen) was added and incubated at room temperature for 25 min. The cells in the six-well plate were washed with medium lacking serum. Fresh medium lacking serum was added (1 ml), and 25 min later, 0.5 ml was removed from each well and replaced by 0.5 ml of DNA/Lipofectamine, added as droplets distributed over the whole well. Plates were incubated for 3 h at 37°C. To plate cells for imaging, they were washed with 2 ml of PBS, and then 400 µl of trypsin was added for 5 min (37°C). A 3-ml amount of complete medium was added, and cells were pipetted up and down 20 times. A 1-ml amount of this was added to a glass-bottom 35-mm dish (MatTek, Ashland, MA) coated with fibronectin, and an additional 1 ml of medium was added. Cells were then grown for ~1 d at 37°C. The medium was replaced with 2 ml of Ham's F-12 medium plus 4% FCS before imaging. For fibronectin coating of MatTek dishes, 300 µl of 5 µg/ml fibronectin (Sigma-Aldrich) in PBS was added to the center of a MatTek dish and incubated for 1 h at 37°C. This was then washed with PBS.

Mouse cortical cultures

Primary cortical neurons were prepared as described previously (Dajas-Bailador *et al.*, 2008) with minor modifications. In brief, mouse cortices were dissected from C57/BL6 embryonic day 17 mice and carefully triturated, and the cell suspension was plated onto poly-L-ornithine–coated culture plates. Neurons were cultured in Neurobasal medium (Invitrogen) supplemented with 5 mM glutamine and 2% B-27 supplement for a maximum of 6–7 d. Cytochalasin D was used for 5 h (10 µg/ml). Transfections of cortical neurons

were carried out 24 h after plating using Lipofectamine 2000 according to manufacturer's instructions. We used *mRFP-EB3* (from Christoph Ballestrem, The University of Manchester, UK; Alves-Silva *et al.*, 2012) and *GFP-CLIP-170* (derived from a rat brain cDNA, *AJ237670*; Akhmanova *et al.*, 2001), both in pEGFP-C1 vector (Clontech).

To assess CLIP-170 isoform expression, RNA was prepared from mouse cortical cultures after 2 or 13 DIV using the TRIzol extraction method. cDNAs were first synthesized using the respective reverse primers (Supplemental Table S2), and SuperScript II Reverse Transcriptase. We used 490 ng of RNA from 13 DIV or 560 ng RNA from 2 DIV. The cDNAs were used as templates for PCR.

Fixation and antibody stainings

Primary fly neurons were fixed in 4% paraformaldehyde (PFA) in 0.05 M phosphate buffer (PB; pH 7–7.2) for 30 min at room temperature or for 10 min in +TIP fix (90% methanol, 3% formaldehyde, 5 mM sodium carbonate, pH 9; stored at –80°C and added ice cold to the cells; Rogers *et al.*, 2002). Mammalian cells were treated with either +TIP fix or a combined fixation (–20°C cold methanol with 1 mM ethylene glycol tetraacetic acid [EGTA] was added and kept on for 10 min at room temperature, followed by 20 min 4% PFA in 0.05 M phosphate buffer, pH 7–7.2, at room temperature; Coquelle *et al.*, 2002; Minami *et al.*, 2010). Stage 16 embryos or late third-instar larvae were dissected flat in 0.2 M PBS as explained elsewhere (Budnik *et al.*, 2006) and fixed with 4% PFA in PB for 1 h.

Antibody staining and washes were performed with PBS with 0.3% Triton-X. Staining reagents were as follows: anti-tubulin (clone DM1A, mouse, 1:1000, Sigma-Aldrich; alternatively, clone YL1/2, rat, 1:500; Millipore Bioscience Research Reagents, Billerica, MA) anti-DmEB1 (rabbit, 1:2000; Elliott *et al.*, 2005); anti-FasII (clone ID4, mouse, 1:20; Developmental Studies Hybridoma Bank [DSHB], Iowa City, IA); anti-GFP (goat, 1:500; Abcam); Cy3-conjugated anti-horseradish peroxidase (HRP; goat, 1:100; Jackson ImmunoResearch, Bar Harbor, ME) anti-synapsin (SYNORF1 3C11, mouse, 1:10; DSHB); anti-CLIP-170 (polyclonal sc-25613, 1:100; Santa Cruz Biotechnology, Dallas, TX) anti-CLIP-190 (rabbit, 1:1000; Dzhindzhev *et al.*, 2005), anti-APC1 (rabbit, 1:1000; Yashi Ahmed, Dartmouth; Hayashi, 1997), anti–myosin-VI (clone 3943, rabbit, 1:100, J. Kendrick-Jones, University of Cambridge, UK), anti-dMyoVI (clone 3C7, mouse, 1:20; K. Miller; Kellerman and Miller, 1992), anti-Lis-1 (rabbit, 1:500; Beat Suter, University of Bern, Switzerland); and fluorescein isothiocyanate (FITC)–, Cy3-, or Cy5-conjugated secondary antibodies (donkey, purified, 1:100 to 1:200; Jackson ImmunoResearch). F-actin was stained with tetramethylrhodamine isothiocyanate/Alexa 647–, FITC-, or Atto 647N–conjugated phalloidin (1:100 or 1:500; Invitrogen and Sigma-Aldrich). Specimens were embedded in Vectashield.

Standard documentation was performed with AxioCam monochrome digital cameras (Carl Zeiss, Oberkochen, Germany) mounted on BX50WI or BX51 (Olympus, Tokyo, Japan) compound fluorescent microscopes. *Z*-stacks of embryonic CNSs were taken with a Leica DM6000 B microscope and extracted with MM AF Premier software (Wetzlar, Germany).

Live imaging

Time-lapse imaging of cultured primary neurons (in Schneider's/FCS) and the embryonic nervous system (in PB) was performed on a Delta Vision RT (Applied Precision, Little Chalfont, UK) restoration microscope using a 100 ×/1.3 Ph3 Uplan Fl objective and the Sedat filter set (Chroma [Bellows Falls, VT] 89000). The images were collected using a CoolSNAP HQ (Photometrics, Tucson, AZ) camera. The temperature control was set to 26°C. For LysoTracker experiments, cells grown for 6 h at 26°C were incubated with 200 nM LysoTracker Red DND-99 (Life Technologies) in culture medium for 20 min and then washed three times with cell culture medium. After washes, cells were incubated for 1 h at 26°C. Time-lapse movies were constructed from images taken every 4 s for 4 min. To analyze lysosome dynamics, lysosomes were tracked manually using the "manual tracking" plug-in for ImageJ (National Institutes of Health, Bethesda, MD).

For live imaging of the embryonic nervous system, preparations were made in 35-mm glass-bottom dishes (MatTek). After dissection, embryos were turned upside down and flattened onto the glass so that the exposed nervous system was in contact with the cover slip through which it could be imaged.

For live imaging of hemocytes or dorsal closure in embryos, dechorionated stage 14/15 embryos were mounted in Voltalef oil on a gas-permeable culture dish (Greiner Lumox; Sigma-Aldrich), and a glass coverslip was placed on top through which they were imaged (Stramer *et al.*, 2010). To analyze hemocytes, the ventral side of embryos was imaged, and for dorsal closure, the dorsal side. Imaging was performed at 25°C using a CSUX1 spinning disk confocal unit (Yokagawa, Tokyo, Japan) on a Zeiss AxioObserver Z1 microscope with a Zeiss alpha Pln Apo 63×/1.46 oil objective, Evolve electron-multiplying charge-coupled device camera (Photometrics), and motorized XYZ stage (ASI). The 488- and 561-nm lasers were controlled using an acousto-optic tunable filter through the laser stack (Intelligent Imaging Innovations, Denver, CO). SlideBook software (Intelligent Imaging Innovations) was used to capture an image every second. Images were exported as TIF files and analyzed on ImageJ.

Image analysis and statistics

For the analysis of *Drosophila* primary neurons, we used two well-established parameters (Sánchez-Soriano *et al.*, 2010; Alves-Silva *et al.*, 2012): axon length (from cell body to growth cone tip) and the degree of MT disorganization in axons. To analyze the strength of comets, the maximum gray value for comets was taken, from which the background intensity was subtracted. From this, a mean value was calculated. Analysis of MT dynamics using EB1::GFP was carried out as described previously (Alves-Silva *et al.*, 2012). For the analysis of motoraxons in stage 16 embryos, the dorsal extent of Fas2-labeled motor nerves relative to HRP-labeled peripheral landmarks was measured (Bottenberg *et al.*, 2009). For the analysis of late larval neuromuscular junctions, the lengths of terminals divided by muscle lengths was determined for muscles VL3/4 and muscle LL of segments A2 and A3 (muscle nomenclature according to Bate, 1993). All length measurements were carried out with ImageJ. For statistical analyses, Kruskal–Wallis one-way analysis of variance (ANOVA) on ranks followed by Mann–Whitney rank sum test (indicated as p_{MW}) were used to compare groups, and χ^2 tests (indicated as p_{X2}) were used to compare percentages.

GFP-trap and Western blotting

Schneider S2 cells from *Drosophila* were cultured using standard methods (Rogers *et al.*, 2002). CLIP-190 fragment plasmids were transfected into 5-ml cultures using Effectene reagent according to manufacturer's instructions (Qiagen, Venlo, Netherlands) and expression was induced with 0.7 mM $CuSO_4$ for 48 h. Cells were spun down at 500 × *g* for 5 min and then resuspended in 500 µl of lysis buffer (25 mM Tris, pH 7.6, 150 mM NaCl, 1 mM dithiothreitol, 1 mM phenylmethylsulfonyl fluoride, 1× cOmplete Mini

Protease Inhibitor [Roche], 15 mM $NaVO_4$, 10 mM *p*-nitrophenyl phosphate, 1 μM okadaic acid, and 0.5% Triton X-100). After 30 min of incubation on ice, lysate was cleared by centrifugation at 13,000 rpm for 30 min at 0°C. A 40-μl amount of GFP-Trap magnetic bead solution (Chromotek, Atlanta, GA) was washed three times with 500 μl of lysis buffer. Cleared cell extract was added to beads and incubated for 2 h at 4°C. Beads were washed times for 10 min with lysis buffer before boiling in sample buffer. Samples were run on an SDS gel and immunoblotted with anti-dMyoVI (clone 3C7, mouse, 1:5; K. Miller) and anti-GFP (A11122, rabbit, 1:500; Life Technologies).

ACKNOWLEDGMENTS

We thank Juliana Alves-Silva and Tom H. Millard for invaluable help with live in vivo imaging of hemocytes and dorsal closure, Niels Galjart for very helpful comments on the manuscript, Frank Bradke, Dorothee Neukirchen, and Anna Akhmanova for kindly providing CLIP-170 constructs, Kathryn Miller for sharing anti-Jar antiserum and *UAS-GFP-jar* fly stocks, Tom Millard, David van Vactor, Mark Peifer, and Peter Kolodziej for sending further fly stocks, John Kendrick-Jones for antisera to mouse myosin-VI, Natalia Sánchez-Soriano for training and continuous help and advice, Sanjai Patel for his help with fly work and larval dissections, Peter Stanley for providing RNA from cultured mouse cortical neurons, and Yutaka Matsubayashi for use of his ImageJ plug-in for blind image analysis. This work was made possible through Biotechnology and Biological Sciences Research Council (BBSRC; BB/I002448/1 and BB/L000717/1) and Wellcome Trust (097820/Z/11/B) support to A.P., Medical Research Council support to F.D.-B. (G0900584), a BBSRC studentship to R.B. (BB/D526561/1), Manchester Faculty of Life Sciences and parent support to Y.Q., and a Wellcome Trust Senior Fellowship to H.O. (081849, 098030, 092076). The Bioimaging Facility microscopes used in this study were purchased with grants from the BBSRC, the Wellcome Trust, and the University of Manchester Strategic Fund, and the Fly Facility was supported by funds from the University of Manchester and the Wellcome Trust (087742/Z/08/Z). Stocks obtained from the Bloomington *Drosophila* Stock Center (supported by National Institutes of Health Award P40OD018537) were used in this study.

REFERENCES

Abe TK, Honda T, Takei K, Mikoshiba K, Hoffman-Kim D, Jay DG, Kuwano R (2008). Dynactin is essential for growth cone advance. Biochem Biophys Res Commun 372, 418–422.

Ahmad FJ, He Y, Myers KA, Hasaka TP, Francis F, Black MM, Baas PW (2006). Effects of dynactin disruption and dynein depletion on axonal microtubules. Traffic 7, 524–537.

Ahmed Y, Hayashi S, Levine A, Wieschaus E (1998). Regulation of armadillo by a Drosophila APC inhibits neuronal apoptosis during retinal development. Cell 93, 1171–1182.

Akhmanova A, Hoogenraad CC, Drabek K, Stepanova T, Dortland B, Verkerk T, Vermeulen W, Burgering BM, De Zeeuw CI, Grosveld F, Galjart N (2001). Clasps are CLIP-115 and -170 associating proteins involved in the regional regulation of microtubule dynamics in motile fibroblasts. Cell 104, 923–935.

Akhmanova A, Mausset-Bonnefont AL, van Cappellen W, Keijzer N, Hoogenraad CC, Stepanova T, Drabek K, van der Wees J, Mommaas M, Onderwater J, *et al.* (2005). The microtubule plus-end-tracking protein CLIP-170 associates with the spermatid manchette and is essential for spermatogenesis. Genes Dev 19, 2501–2515.

Akhmanova A, Steinmetz MO (2008). Tracking the ends: a dynamic protein network controls the fate of microtubule tips. Nat Rev Mol Cell Biol 9, 309–322.

Akhmanova A, Steinmetz MO (2010). Microtubule +TIPs at a glance. J Cell Sci 123, 3415–3419.

Akong K, McCartney BM, Peifer M (2002). *Drosophila* APC2 and APC1 have overlapping roles in the larval brain despite their distinct intracellular localizations. Dev Biol 250, 71–90.

Allan VJ (2011). Cytoplasmic dynein. Biochem Soc Trans 39, 1169–1178.

Alves-Silva J, Sánchez-Soriano N, Beaven R, Klein M, Parkin J, Millard T, Bellen H, Venken KJT, Ballestrem C, Kammerer RA, Prokop A (2012). Spectraplakins promote microtubule-mediated axonal growth by functioning as structural microtubule-associated proteins and EB1-dependent +TIPs (tip interacting proteins). J Neurosci 32, 9143–9158.

Arnal I, Heichette C, Diamantopoulos GS, Chretien D (2004). CLIP-170/tubulin-curved oligomers coassemble at microtubule ends and promote rescues. Curr Biol 14, 2086–2095.

Bate M (1993). The mesoderm and its derivatives. In: The Development of *Drosophila melanogaster*, Vol. 2, ed. M Bate and A Martínez Arias, Cold Spring Harbor, NY: Cold Spring Harbor Laboratory Press, 1013–1090.

Bottenberg W, Sánchez-Soriano N, Alves-Silva J, Hahn I, Mende M, Prokop A (2009). Context-specific requirements of functional domains of the Spectraplakin Short stop *in vivo*. Mech Dev 26, 489–502.

Budnik V, Gorczyca M, Prokop A (2006). Selected methods for the anatomical study of *Drosophila* embryonic and larval neuromuscular junctions. Int Rev Neurobiol 75, 323–374.

Buss F, Kendrick-Jones J (2008). How are the cellular functions of myosin VI regulated within the cell? Biochem Biophys Res Commun 369, 165–175.

Campos-Ortega JA, Hartenstein V (1997). The Embryonic Development of *Drosophila melanogaster*, Berlin: Springer-Verlag.

Chilton J, Gordon-Weeks P (2007). Role of microtubules and MAPs during neuritogenesis. In: Intracellular Mechanisms for Neuritogenesis, ed. I de Curtis, New York: Springer, 57–88.

Conde C, Caceres A (2009). Microtubule assembly, organization and dynamics in axons and dendrites. Nat Rev Neurosci 10, 319–332.

Coquelle FM, Caspi M, Cordelieres FP, Dompierre JP, Dujardin DL, Koifman C, Martin P, Hoogenraad CC, Akhmanova A, Galjart N, *et al.* (2002). LIS1, CLIP-170's key to the dynein/dynactin pathway. Mol Cell Biol 22, 3089–3102.

Cramer LP (2000). Myosin VI: roles for a minus end-directed actin motor in cells. J Cell Biol 150, F121–F126.

Dajas-Bailador F, Jones EV, Whitmarsh AJ (2008). The JIP1 scaffold protein regulates axonal development in cortical neurons. Curr Biol 18, 221–226.

Dent EW, Gupton SL, Gertler FB (2011). The growth cone cytoskeleton in axon outgrowth and guidance. Cold Spring Harb Perspect Biol 3, a001800.

De Zeeuw CI, Hoogenraad CC, Goedknegt E, Hertzberg E, Neubauer A, Grosveld F, Galjart N (1997). CLIP-115, a novel brain-specific cytoplasmic linker protein, mediates the localization of dendritic lamellar bodies. Neuron 19, 1187–1199.

Dix CI, Soundararajan HC, Dzhindzhev NS, Begum F, Suter B, Ohkura H, Stephens E, Bullock SL (2013). Lissencephaly-1 promotes the recruitment of dynein and dynactin to transported mRNAs. J Cell Biol 202, 479–494.

Dzhindzhev NS, Rogers SL, Vale RD, Ohkura H (2005). Distinct mechanisms govern the localisation of Drosophila CLIP-190 to unattached kinetochores and microtubule plus-ends. J Cell Sci 118, 3781–3790.

Elliott SL, Cullen CF, Wrobel N, Kernan MJ, Ohkura H (2005). EB1 is essential during *Drosophila* development and plays a crucial role in the integrity of chordotonal mechanosensory organs. Mol Biol Cell 16, 891–901.

Etienne-Manneville S (2010). From signaling pathways to microtubule dynamics: the key players. Curr Opin Cell Biol 22, 104–111.

Feinstein SC, Wilson L (2005). Inability of tau to properly regulate neuronal microtubule dynamics: a loss-of-function mechanism by which tau might mediate neuronal cell death. Biochim Biophys Acta 1739, 268–279.

Finan D, Hartman MA, Spudich JA (2011). Proteomics approach to study the functions of Drosophila myosin VI through identification of multiple cargo-binding proteins. Proc Natl Acad Sci USA 108, 5566–5571.

Garrido JJ, Simon D, Varea O, Wandosell F (2007). GSK3 alpha and GSK3 beta are necessary for axon formation. FEBS Lett 581, 1579–1586.

Gepner J, Li M, Ludmann S, Kortas C, Boylan K, Iyadurai SJ, McGrail M, Hays TS (1996). Cytoplasmic dynein function is essential in Drosophila melanogaster. Genetics 142, 865–878.

Goodson HV, Skube SB, Stalder R, Valetti C, Kreis TE, Morrison EE, Schroer TA (2003). CLIP-170 interacts with dynactin complex and the APC-binding protein EB1 by different mechanisms. Cell Motil Cytoskeleton 55, 156–173.

Grabham PW, Seale GE, Bennecib M, Goldberg DJ, Vallee RB (2007). Cytoplasmic dynein and LIS1 are required for microtubule advance during growth cone remodeling and fast axonal outgrowth. J Neurosci 27, 5823–5834.
Gupta KK, Joyce MV, Slabbekoorn AR, Zhu ZC, Paulson BA, Boggess B, Goodson HV (2010). Probing interactions between CLIP-170, EB1, and microtubules. J Mol Biol 395, 1049–1062.
Gupta KK, Paulson BA, Folker ES, Charlebois B, Hunt AJ, Goodson HV (2009). Minimal plus-end tracking unit of the cytoplasmic linker protein CLIP-170. J Biol Chem 284, 6735–6742.
Halfon MS, Gisselbrecht S, Lu J, Estrada B, Keshishian H, Michelson AM (2002). New fluorescent protein reporters for use with the Drosophila Gal4 expression system and for vital detection of balancer chromosomes. Genesis 34, 135–138.
Hasson T (2003). Myosin VI: two distinct roles in endocytosis. J Cell Sci 116, 3453–3461.
Hayashi S (1997). A Drosophila homolog of the tumor suppressor gene adenomatous polyposis coli down-regulates beta-catenin but its zygotic expression is not essential for the regulation of Armadillo. 94, 242–247.
He Y, Francis F, Myers KA, Yu W, Black MM, Baas PW (2005). Role of cytoplasmic dynein in the axonal transport of microtubules and neurofilaments. J Cell Biol 168, 697–703.
Hur EM, Saijilafu, Lee BD, Kim SJ, Xu WL, Zhou FQ (2011). GSK3 controls axon growth via CLASP-mediated regulation of growth cone microtubules. Genes Dev 25, 1968–1981.
Inoue YH, do Carmo Avides M, Shiraki M, Deak P, Yamaguchi M, Nishimoto Y, Matsukage A, Glover DM (2000). Orbit, a novel microtubule-associated protein essential for mitosis in Drosophila melanogaster. J Cell Biol 149, 153–166.
Kapitein LC, van Bergeijk P, Lipka J, Keijzer N, Wulf PS, Katrukha EA, Akhmanova A, Hoogenraad CC (2013). Myosin-v opposes microtubule-based cargo transport and drives directional motility on cortical actin. Curr Biol 23, 828–834.
Kellerman KA, Miller KG (1992). An unconventional myosin heavy chain gene from Drosophila melanogaster. J Cell Biol 119, 823–834.
Kisiel M, McKenzie K, Stewart B (2014). Localization and mobility of synaptic vesicles in *myosin VI* mutants of *Drosophila*. PLoS One 9, e102988.
Koester MP, Muller O, Pollerberg GE (2007). Adenomatous polyposis coli is differentially distributed in growth cones and modulates their steering. J Neurosci 27, 12590–12600.
Kolodziej PA, Jan LY, Jan YN (1995). Mutations that affect the length, fasciculation, or ventral orientation of specific sensory axons in the *Drosophila* embryo. Neuron 15, 273–286.
Komarova YA, Akhmanova AS, Kojima S, Galjart N, Borisy GG (2002). Cytoplasmic linker proteins promote microtubule rescue in vivo. J Cell Biol 159, 589–599.
Landgraf M, Sánchez-Soriano N, Technau GM, Urban J, Prokop A (2003). Charting the *Drosophila* neuropile: a strategy for the standardised characterisation of genetically amenable neurites. Dev Biol 260, 207–225.
Lansbergen G, Komarova Y, Modesti M, Wyman C, Hoogenraad CC, Goodson HV, Lemaitre RP, Drechsel DN, van Munster E, Gadella TW Jr, *et al*. (2004). Conformational changes in CLIP-170 regulate its binding to microtubules and dynactin localization. J Cell Biol 166, 1003–1014.
Lantz VA, Miller KG (1998). A class VI unconventional myosin is associated with a homologue of a microtubule-binding protein, cytoplasmic linker protein-170, in neurons and at the posterior pole of *Drosophila* embryos. J Cell Biol 140, 897–910.
Lazarus JE, Moughamian AJ, Tokito MK, Holzbaur EL (2013). Dynactin subunit p150(Glued) is a neuron-specific anti-catastrophe factor. PLoS Biol 11, e1001611.
Lee H, Engel U, Rusch J, Scherrer S, Sheard K, Van Vactor D (2004). The microtubule plus end tracking protein Orbit/MAST/CLASP acts downstream of the tyrosine kinase Abl in mediating axon guidance. Neuron 42, 913–926.
Lee HS, Komarova YA, Nadezhdina ES, Anjum R, Peloquin JG, Schober JM, Danciu O, van Haren J, Galjart N, Gygi SP, *et al*. (2010). Phosphorylation controls autoinhibition of cytoplasmic linker protein-170. Mol Biol Cell 21, 2661–2673.
Lewis P, Lentz TL (1998). Rabies virus entry into cultured rat hippocampal neurons. J Neurocytol 27, 559–573.
Lin HP, Chen HM, Wei SY, Chen LY, Chang LH, Sun YJ, Huang SY, Hsu JC (2007). Cell adhesion molecule Echinoid associates with unconventional myosin VI/Jaguar motor to regulate cell morphology during dorsal closure in *Drosophila*. Dev Biol 311, 423–433.
Liu Z, Steward R, Lu LQ (2000). Drosophila Lis1 is required for neuroblast proliferation, dendritic elaboration and axonal transport. Nat Cell Biol 2, 776–783.
Lomakin AJ, Semenova I, Zaliapin I, Kraikivski P, Nadezhdina E, Slepchenko BM, Akhmanova A, Rodionov V (2009). CLIP-170-dependent capture of membrane organelles by microtubules initiates minus-end directed transport. Dev Cell 17, 323–333.
Loubery S, Delevoye C, Louvard D, Raposo G, Coudrier E (2012). Myosin VI regulates actin dynamics and melanosome biogenesis. Traffic 13, 665–680.
Lowery LA, Lee H, Lu C, Murphy R, Obar RA, Zhai B, Schedl M, Van Vactor D, Zhan Y (2010). Parallel genetic and proteomic screens identify Msps as a CLASP-Abl pathway interactor in *Drosophila*. Genetics 185, 1311–1325.
Luo L, Liao YJ, Jan LY, Jan YN (1994). Distinct morphogenetic functions of similar small GTPases: *Drosophila* Drac1 is involved in axonal outgrowth and myoblast fusion. Genes Dev 8, 1787–1802.
Marrone AK, Kucherenko MM, Rishko VM, Shcherbata HR (2011). New Dystrophin/Dystroglycan interactors control neuron behavior in Drosophila eye. BMC Neurosci 12, 93.
Marx A, Godinez WJ, Tsimashchuk V, Bankhead P, Rohr K, Engel U (2013). Xenopus cytoplasmic linker-associated protein 1 (XCLASP1) promotes axon elongation and advance of pioneer microtubules. Mol Biol Cell 24, 1544–1558.
Mathe E, Inoue YH, Palframan W, Brown G, Glover DM (2003). Orbit/Mast, the CLASP orthologue of Drosophila, is required for asymmetric stem cell and cystocyte divisions and development of the polarised microtubule network that interconnects oocyte and nurse cells during oogenesis. Development 130, 901–915.
Mattie FJ, Stackpole MM, Stone MC, Clippard JR, Rudnick DA, Qiu Y, Tao J, Allender DL, Parmar M, Rolls MM (2010). Directed microtubule growth, +TIPs, and kinesin-2 are required for uniform microtubule polarity in dendrites. Curr Biol 20, 2169–2177.
McCartney BM, Price MH, Webb RL, Hayden MA, Holot LM, Zhou M, Bejsovec A, Peifer M (2006). Testing hypotheses for the functions of APC family proteins using null and truncation alleles in Drosophila. Development 133, 2407–2418.
Miedema M (2007). Cytoplasmic linker proteins: keeping in shape by regulating the cytoskeleton Erasmus University Rotterdam. Available at http://hdl.handle.net/1765/9464 (accessed 15 March 2015).
Millo H, Leaper K, Lazou V, Bownes M (2004). Myosin VI plays a role in cell-cell adhesion during epithelial morphogenesis. Mech Dev 121, 1335–1351.
Mimori-Kiyosue Y, Grigoriev I, Lansbergen G, Sasaki H, Matsui C, Severin F, Galjart N, Grosveld F, Vorobjev I, Tsukita S, Akhmanova A (2005). CLASP1 and CLASP2 bind to EB1 and regulate microtubule plus-end dynamics at the cell cortex. J Cell Biol 168, 141–153.
Minami A, Mizutani K, Waseda M, Kajita M, Miyata M, Ikeda W, Takai Y (2010). Necl-5/PVR enhances PDGF-induced attraction of growing microtubules to the plasma membrane of the leading edge of moving NIH3T3 cells. Genes Cells 15, 1123–1135.
Mishima M, Maesaki R, Kasa M, Watanabe T, Fukata M, Kaibuchi K, Hakoshima T (2007). Structural basis for tubulin recognition by cytoplasmic linker protein 170 and its autoinhibition. Proc Natl Acad Sci USA 104, 10346–10351.
Morrison JK, Miller KG (2008). Genetic characterization of the Drosophila jaguar322 mutant reveals that complete myosin VI loss of function is not lethal. Genetics 179, 711–716.
Moughamian AJ, Osborn GE, Lazarus JE, Maday S, Holzbaur EL (2013). Ordered recruitment of dynactin to the microtubule plus-end is required for efficient initiation of retrograde axonal transport. J Neurosci 33, 13190–13203.
Murphey RK, Caruccio PC, Getzinger M, Westgate PJ, Phillis RW (1999). Dynein-dynactin function and sensory axon growth during *Drosophila* metamorphosis: A role for retrograde motors. Dev Biol 209, 86–97.
Nakano A, Kato H, Watanabe T, Min K-D, Yamazaki S, Asano Y, Seguchi O, Higo S, Shintani Y, Asanuma H, *et al*. (2010). AMPK controls the speed of microtubule polymerization and directional cell migration through CLIP-170 phosphorylation. Nat Cell Biol 12, 583–590.
Neukirchen D, Bradke F (2011). Cytoplasmic linker proteins regulate neuronal polarization through microtubule and growth cone dynamics. J Neurosci 31, 1528–1538.
Noguchi T, Lenartowska M, Miller KG (2006). Myosin VI stabilizes an actin network during Drosophila spermatid individualization. Mol Biol Cell 17, 2559–2571.

Näthke IS, Adams CL, Polakis P, Sellin JH, Nelson WJ (1996). The adenomatous polyposis coli tumor suppressor protein localizes to plasma membrane sites involved in active cell migration. J Cell Biol 134, 165–179.
Papoulas O, Hays TS, Sisson JC (2005). The golgin Lava lamp mediates dynein-based Golgi movements during Drosophila cellularization. Nat Cell Biol 7, 612–618.
Perez F, Diamantopoulos GS, Stalder R, Kreis TE (1999). CLIP-170 highlights growing microtubule ends in vivo. Cell 96, 517–527.
Phichith D, Travaglia M, Yang Z, Liu X, Zong AB, Safer D, Sweeney HL (2009). Cargo binding induces dimerization of myosin VI. Proc Natl Acad Sci USA 106, 17320–17324.
Pierre P, Scheel J, Rickard JE, Kreis TE (1992). CLIP-170 links endocytic vesicles to microtubules. Cell 70, 887–900.
Prokop A (2013). The intricate relationship between microtubules and their associated motor proteins during axon growth and maintenance. Neural Dev 8, 17.
Prokop A, Beaven R, Qu Y, Sánchez-Soriano N (2013). Using fly genetics to dissect the cytoskeletal machinery of neurons during axonal growth and maintenance. J Cell Sci 126, 2331–2341.
Prokop A, Küppers-Munther B, Sánchez-Soriano N (2012). Using primary neuron cultures of *Drosophila* to analyse neuronal circuit formation and function. In: The Making and Un-Making of Neuronal Circuits in *Drosophila*, Vol. 69, ed. BA Hassan, New York: Humana Press, 225–247.
Prokop A, Meinertzhagen IA (2006). Development and structure of synaptic contacts in *Drosophila*. Semin Cell Dev Biol 17, 20–30.
Rickard JE, Kreis TE (1990). Identification of a novel nucleotide-sensitive microtubule-binding protein in HeLa cells. J Cell Biol 110, 1623–1633.
Roberts DM, Pronobis MI, Poulton JS, Kane EG, Peifer M (2012). Regulation of Wnt signaling by the tumor suppressor adenomatous polyposis coli does not require the ability to enter the nucleus or a particular cytoplasmic localization. Mol Biol Cell 23, 2041–2056.
Rogers SL, Rogers GC, Sharp DJ, Vale RD (2002). Drosophila EB1 is important for proper assembly, dynamics, and positioning of the mitotic spindle. J Cell Biol 158, 873–884.
Rogers GC, Rusan NM, Peifer M, Rogers SL (2008). A multicomponent assembly pathway contributes to the formation of acentrosomal microtubule arrays in interphase Drosophila cells. Mol Biol Cell 19, 3163–3178.
Rusan NM, Akong K, Peifer M (2008). Putting the model to the test: are APC proteins essential for neuronal polarity, axon outgrowth, and axon targeting? J Cell Biol 183, 203–212.
Sahlender DA, Roberts RC, Arden SD, Spudich G, Taylor MJ, Luzio JP, Kendrick-Jones J, Buss F (2005). Optineurin links myosin VI to the Golgi complex and is involved in Golgi organization and exocytosis. J Cell Biol 169, 285–295.
Sánchez-Soriano N, Gonçalves-Pimentel C, Beaven R, Haessler U, Ofner L, Ballestrem C, Prokop A (2010). *Drosophila* growth cones: a genetically tractable platform for the analysis of axonal growth dynamics. Dev Neurobiol 70, 58–71.
Sánchez-Soriano N, Prokop A (2005). The influence of pioneer neurons on a growing motor nerve in *Drosophila* requires the neural cell adhesion molecule homolog FasciclinII. J Neurosci 25, 78–87.
Sánchez-Soriano N, Tear G, Whitington P, Prokop A (2007). *Drosophila* as a genetic and cellular model for studies on axonal growth. Neural Dev 2, 9.
Sánchez-Soriano N, Travis M, Dajas-Bailador F, Goncalves-Pimentel C, Whitmarsh AJ, Prokop A (2009). Mouse ACF7 and *Drosophila* Short stop modulate filopodia formation and microtubule organisation during neuronal growth. J Cell Sci 122, 2534–2542.
Sattler R, Xiong Z, Lu WY, MacDonald JF, Tymianski M (2000). Distinct roles of synaptic and extrasynaptic NMDA receptors in excitotoxicity. J Neurosci 20, 22–33.
Siller KH, Serr M, Steward R, Hays TS, Doe CQ (2005). Live imaging of Drosophila brain neuroblasts reveals a role for Lis1/dynactin in spindle assembly and mitotic checkpoint control. Mol Biol Cell 16, 5127–5140.
Sisson JC, Field C, Ventura R, Royou A, Sullivan W (2000). Lava lamp, a novel peripheral golgi protein, is required for Drosophila melanogaster cellularization. J Cell Biol 151, 905–918.
Stepanova T, Slemmer J, Hoogenraad CC, Lansbergen G, Dortland B, De Zeeuw CI, Grosveld F, van Cappellen G, Akhmanova A, Galjart N (2003). Visualization of microtubule growth in cultured neurons via the use of EB3-GFP (end-binding protein 3-green fluorescent protein). J Neurosci 23, 2655–2664.
Stepanova T, Smal I, van Haren J, Akinci U, Liu Z, Miedema M, Limpens R, van Ham M, van der Reijden M, Poot R, *et al*. (2010). History-dependent catastrophes regulate axonal microtubule behavior. Curr Biol 20, 1023–1028.
Stramer B, Moreira S, Millard T, Evans I, Huang CY, Sabet O, Milner M, Dunn G, Martin P, Wood W (2010). Clasp-mediated microtubule bundling regulates persistent motility and contact repulsion in Drosophila macrophages in vivo. J Cell Biol 189, 681–689.
Swan A, Nguyen T, Suter B (1999). Drosophila Lissencephaly-1 functions with Bic-D and dynein in oocyte determination and nuclear positioning. Nat Cell Biol 1, 444–449.
Swiech L, Blazejczyk M, Urbanska M, Pietruszka P, Dortland BR, Malik AR, Wulf PS, Hoogenraad CC, Jaworski J (2011). CLIP-170 and IQGAP1 cooperatively regulate dendrite morphology. J Neurosci 31, 4555–4568.
Tortosa E, Galjart N, Avila J, Sayas CL (2013). MAP1B regulates microtubule dynamics by sequestering EB1/3 in the cytosol of developing neuronal cells. EMBO J 32, 1293–1306.
Tymanskyj SR, Scales TM, Gordon-Weeks PR (2012). MAP1B enhances microtubule assembly rates and axon extension rates in developing neurons. Mol Cell Neurosci 49, 110–119.
Venken KJ, Bellen HJ (2007). Transgenesis upgrades for Drosophila melanogaster. Development 134, 3571–3584.
Votin V, Nelson WJ, Barth AI (2005). Neurite outgrowth involves adenomatous polyposis coli protein and beta-catenin. J Cell Sci 118, 5699–5708.
Weisbrich A, Honnappa S, Jaussi R, Okhrimenko O, Frey D, Jelesarov I, Akhmanova A, Steinmetz MO (2007). Structure-function relationship of CAP-Gly domains. Nat Struct Mol Biol 14, 959–967.
Zhou F-Q, Zhou J, Dedhar S, Wu Y-H, Snider WD (2004). NGF-induced axon growth is mediated by localized inactivation of GSK-3beta and functions of the microtubule plus end binding protein APC. Neuron 42, 897–912.